NOAA TR ERL 219-WPL 18

NOAA Technical Report ERL 219-WPL 18

U.S. DEPARTMENT OF COMMERCE
National Oceanic and Atmospheric Administration
Environmental Research Laboratories

Microwave Emission From Clouds

ED R. WESTWATER

BOULDER, COLO.
JANUARY 1972

IMENTAL RESEARCH LABORATORIES

f the Environmental Research Laboratories is to study the oceans, inland and upper atmosphere, the space environment, and the earth, in search ing needed to provide more useful services in improving man's prospects luenced by the physical environment. Laboratories contributing to these

s Laboratories (ESL): Geomagnetism, seismology, geodesy, and related earth sciences; earthquake processes, internal structure and accurate figure of the Earth, and distribution of the Earth's mass.

Atlantic Oceanographic and Meteorological Laboratories (AOML): Oceanography, with emphasis on the geology and geophysics of ocean basins, oceanic processes, sea-air interactions, hurrican research, and weather modification (Miami, Florida).

Pacific Oceanographic Laboratories (POL): Oceanography; geology and geophysics of the Pacific Basin and margins; oceanic processes and dynamics; tsunami generation, propagation, modification, detection, and monitoring (Seattle, Washington).

Atmospheric Physics and Chemistry Laboratory (APCL): Cloud physics and precipitation; chemical composition and nucleating substances in the lower atmosphere; and laboratory and field experiments toward developing feasible methods of weather modification.

Air Resources Laboratories (ARL): Diffusion, transport, and dissipation of atmospheric contaminants; development of methods for prediction and control of atmospheric pollution (Silver Spring, Maryland).

Geophysical Fluid Dynamics Laboratory (GFDL): Dynamics and physics of geophysical fluid systems; development of a theoretical basis, through mathematical modeling and computer simulation, for the behavior and properties of the atmosphere and the oceans (Princeton, New Jersey).

Research Flight Facility (RFF): Outfits and operates aircraft specially instrumented for research; and meets needs of NOAA and other groups for environmental measurements for aircraft (Miami, Florida).

National Severe Storms Laboratory (NSSL): Tornadoes, squall lines, thunderstorms, and other severe local convective phenomena toward achieving improved methods of forecasting, detecting, and providing advance warnings (Norman, Oklahoma).

Space Environment Laboratory (SEL): Conducts research in solar-terrestrial physics, provides services and technique development in areas of environmental monitoring, forecasting, and data archiving.

Aeronomy Laboratory (AL): Theoretical, laboratory, rocket, and satellite studies of the physical and chemical processes controlling the ionosphere and exosphere of the earth and other planets.

Wave Propagation Laboratory (WPL): Development of new methods for remote sensing of the geophysical environment; special emphasis on propagation of sound waves, and electromagnetic waves at millimeter, infrared, and optical frequencies.

Marine Minerals Technology Center (MMTC): Research into aspects of undersea mining of hard minerals: development of tools and techniques to characterize and monitor the marine mine environment; prediction of the possible effects of marine mining on the environment; development of fundamental mining technology (Tiburon, California).

NATIONAL OCEANIC AND ATMOSPHERIC ADMINISTRATION

BOULDER, COLORADO 80302

U.S. DEPARTMENT OF COMMERCE
Maurice H. Stans, Secretary

NATIONAL OCEANIC AND ATMOSPHERIC ADMINISTRATION
Robert M. White, Administrator

ENVIRONMENTAL RESEARCH LABORATORIES
Wilmot N. Hess, Director

NOAA TECHNICAL REPORT ERL 219-WPL 18

Microwave Emission From Clouds

ED R. WESTWATER

BOULDER, COLO.
January 1972

For sale by the Superintendent of Documents, U. S. Government Printing Office, Washington, D. C. 20402
Price 70 cents

TABLE OF CONTENTS

	Page
ABSTRACT	1
1. INTRODUCTION	1
2. MODEL ATMOSPHERES	2
3. CLEAR ATMOSPHERIC ABSORPTION	8
4. ATTENUATION BY CLOUDS	13
5. EMISSION CALCULATIONS	17
6. SUMMARY AND DISCUSSION	40
7. ACKNOWLEDGMENTS	41
8. REFERENCES	42
APPENDIX A. VALIDITY OF RAYLEIGH APPROXIMATION	
APPENDIX B. ATTENUATION BY CLOUDS AT 15, 31, AND 53 GHz, by J. B. Snider	
APPENDIX C. ABSORPTION BY TWO-COMPONENT ICE-WATER SPHERES IN THE RAYLEIGH REGION	

FIGURE CAPTIONS

Figure 1. Clear atmosphere temperature and humidity models.

Figure 2. Stratiform cloud models.

Figure 3. Thunderstorm models.

Figure 4. Gaseous microwave absorption.

Figure 5. Calculated Rayleigh attenuation for water, ice and two-component ice water spheres.

Figure 6. Dependence of attenuation of two-component spheres on q.

Figure 7. Nadir brightness temperatures for clear atmosphere.

Figure 8. Nadir temperature weighting functions.

Figure 9. Temperature weighting functions for various nadir angles.

Figure 10-15. Effect of water clouds on temperature weighting functions.

Figure 16-18. Nadir brightness for various cloud models.

Figure 19. Opacity for various cloud models.

Figure 20. Nadir brightness for ice clouds above freezing level.

Figure 21. Nadir brightness for two-component clouds above freezing level.

Figure 22. Opacity calculations for various ice-water clouds.

Figure 23. Temperature weighting function for ice clouds above freezing level.

Figure 24. Nadir brightness calculations for various ice-water clouds.

MICROWAVE EMISSION FROM CLOUDS

Ed R. Westwater

Calculations of microwave thermal emission to space from Rayleigh attenuating clouds are given. The emission and attenuation from ice, water, and two-component ice-water spheres are calculated for tropical, arctic, and standard atmospheres with stratiform clouds and thunderstorm liquid water distributions. The effect of clouds on temperature weighting functions is considered. Cumulative distributions of measured attenuation at 15.25, 31.65, and 52.50 GHz are presented. The Rayleigh attenuation from two-component spheres is discussed in detail.

1. INTRODUCTION

The effect of clouds on microwave emission to space is an important consideration in remote sensing of atmospheric and surface parameters by satellites. In this report, we present calculations for a variety of clouds, surface and clear atmospheric models. Cloud attenuation is calculated from the Rayleigh approximation for water, ice, and two-component ice-water spheres.

The organization of this report is: Section 2 contains the cloudy and clear atmospheric models on which subsequent calculations are based. Sections 3 and 4 discuss the methods of calculating clear and cloudy absorption. Section 5 contains calculations of cloud emission, attenuation and of their effect upon temperature weighting functions. The validity of the Rayleigh approximation is discussed in Appendix A, while Appendix C discusses in detail the absorption properties of two-component ice and water spheres. Cumulative distributions of measured attenuation at 15.25, 31.65, and 52.50 GHz are given in Appendix B. These data are based on two weeks of observations at Upolu Point, Hawaii.

2. MODEL ATMOSPHERES

Calculations of microwave brightness presented in Section 5 are based on a variety of clear and cloudy atmospheric models. Three clear atmospheric models were chosen from the 1965 Handbook of Geophysics and Space Environments: (1) 1962 U.S. Standard Atmosphere, (2) Tropical (15°N), and (3) Subarctic (60°N) Winter Cold. These clear reference models are shown in figure 1. In this and the following two figures, the cloud thickness and base heights are in km and the mean cloud density is in g/m^3.

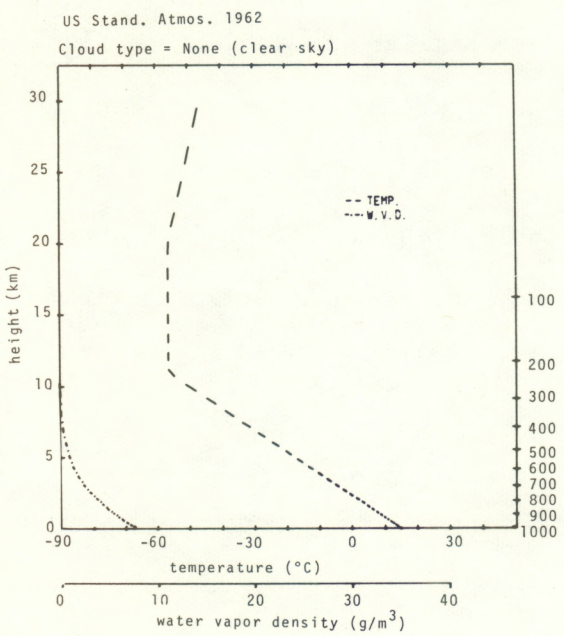

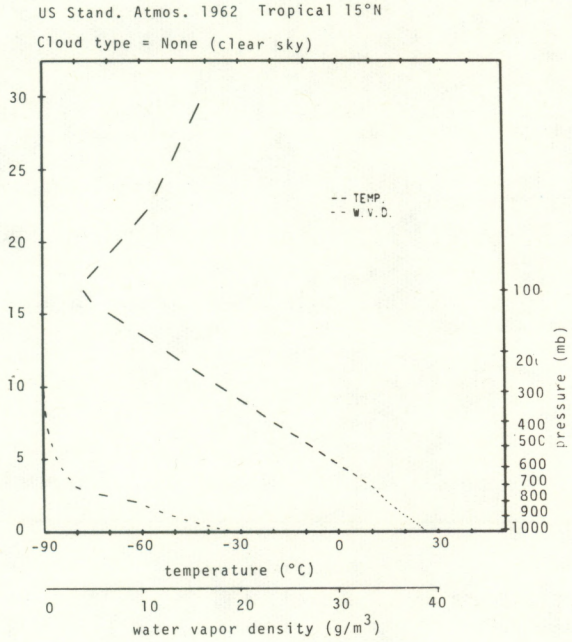

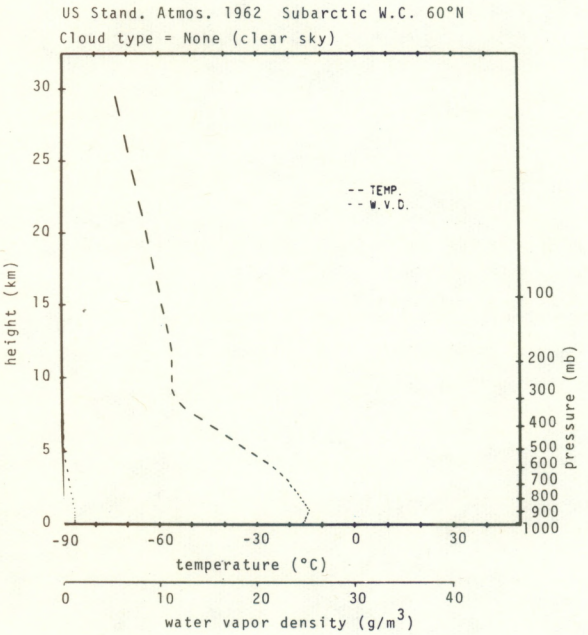

Figure 1. Clear atmosphere temperature and humidity models.

Two distinct types of cloud models were assumed: stratiform clouds [Feigel'son, 1966], and thunderstorms. Stratiform clouds comprise cirrostratus (Cs), altostratus (As), nimbostratus (Ns), stratocumulus (Sc) and stratus (St). Altocumulus (Ac) also have similar physical properties. Table 1 [Feigel'son, 1966] gives average cloud parameters for stratiform clouds. In calculations of cloud thermal emission properties, three stratiform cloud models were chosen from table 1 and are shown in figure 2. In all cloud models the relative humidity is set to 100 percent within the cloud layer.

Table 1. Average Cloud Parameters for Stratiform Clouds.

Cloud form	Layer thickness H, km	Base height km	Average liquid-water content, g/m^3	Average drop radius μ
St	~0.5	0.1-0.7	0.2	5.2
Sc	~0.5	0.5-1.5	0.2-0.3	5.0
Ns-As	2-3	0.1-1	0.3	5.5(6-7)
As	~0.9	2-6	0.17	4.8
Ac	~0.3	2-6	0.1	4.5-5
Ns-As-Cs	5-6	1	-	-
Cs	1.2	6-8	0.03	-

Thunderstorm models were obtained from the Handbook of Geophysics and Space Environments (1965). "Weak", "average" and "strong" thunderstorm models are shown in figure 3. It is assumed that rain

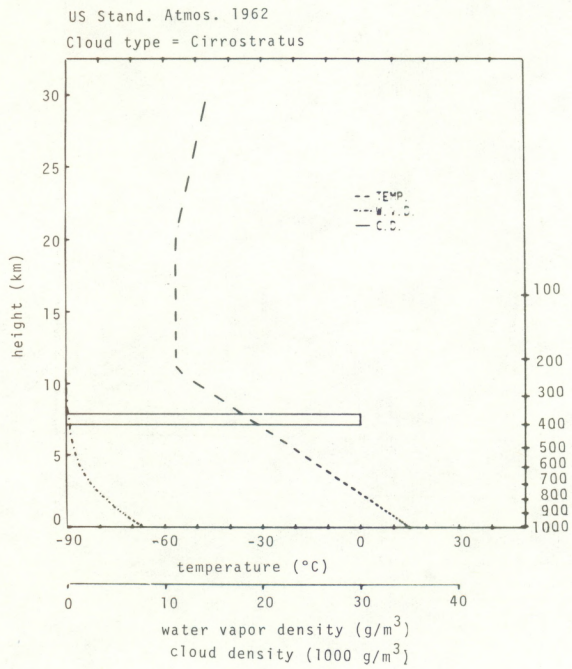

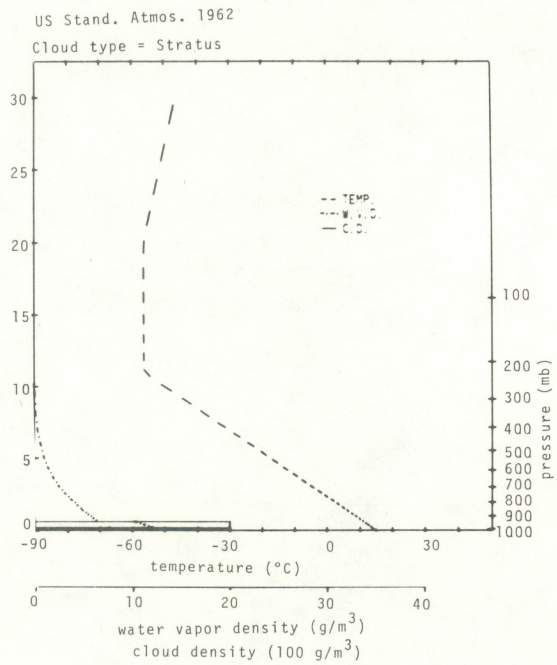

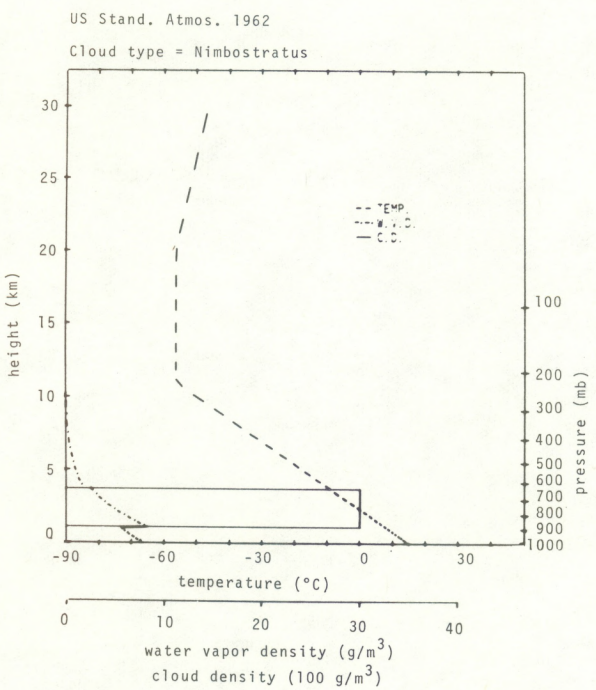

Figure 2. Stratiform cloud models.

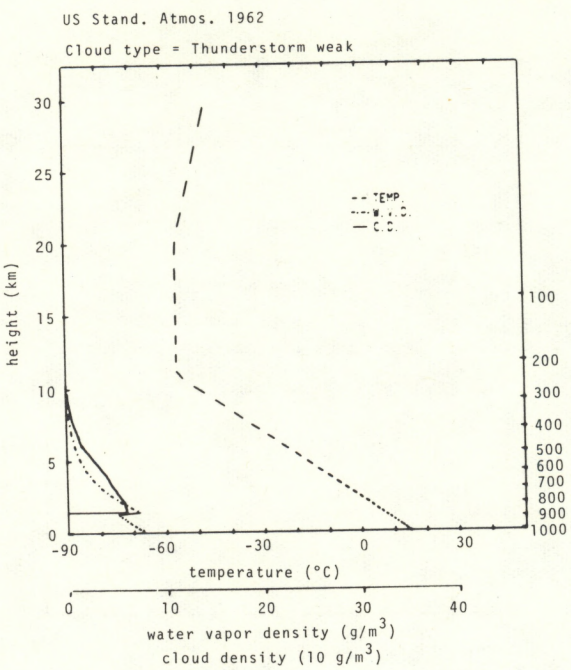

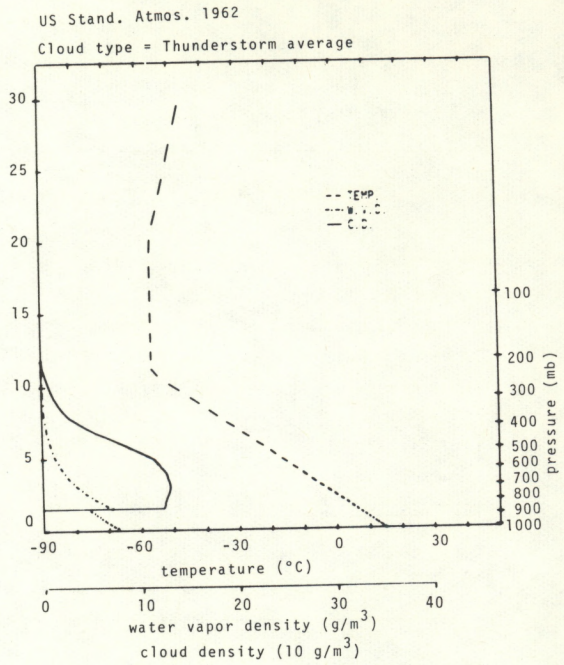

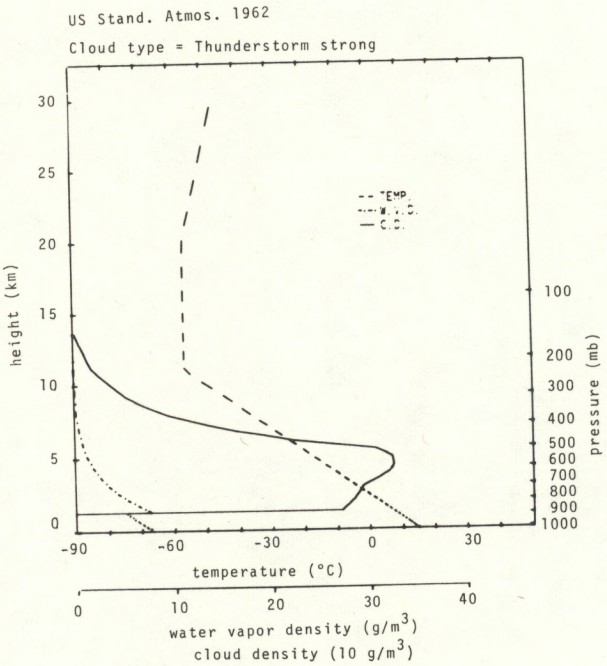

Figure 3. Thunderstorm models.

is absent in the thunderstorm and that the drop size distribution is in the Rayleigh region. (See Appendix A). For drop size distributions characteristic of rain, Deirmendjian [1963] has shown that the exact Mie equations must be used to compute microwave extinction.

3. CLEAR ATMOSPHERIC ABSORPTION

In the earth's atmosphere, gaseous microwave absorption and emission are due primarily to water vapor and oxygen. Absorption from other trace constituents having microwave lines, such as NH_3 and O_3, is relatively small, although emission from O_3 has been observed around 30 GHz [Caton, Welch and Silver, 1967]. A table giving the expected microwave absorption by trace constituents is given by Welch [1968].

Water vapor absorption of microwaves is due to the electric dipole rotational transition $6_{-5} - 5_{-1}$ at 22.235 GHz and to the far wing absorption of sub-millimeter and infrared lines [Van Vleck, 1947a]. This absorption has been measured in the laboratory by Becker and Autler [1946] and in the atmosphere by Staelin [1966], Falcone [1966] and Snider and Westwater [1969]. These measurements give consistent results when interpreted by the Van Vleck theory if a semi-empirical correction is made for the wing contribution of the higher frequency lines. Calculations of water vapor absorption in this report are based on parameters derived from the Becker and Autler data by Westwater [1967]. These equations are

$$\frac{\alpha_w}{\rho} = \left(\frac{318.0}{T}\right)^{5/2} \exp\left(-\frac{644.0}{T} + \frac{644.0}{318.0}\right) \tilde{\nu}^2 C_1 \left\{ \frac{(\Delta\nu/c)_w}{(\tilde{\nu} - \tilde{\nu}_o)^2 + (\frac{\Delta\nu}{c})_w^2} + \frac{(\Delta\nu/c)_w}{(\tilde{\nu} + \tilde{\nu}_o)^2 + (\Delta\nu/c)_w^2} \right\} + \left(\frac{318.0}{T}\right) C_2 \tilde{\nu}^2 \left(\frac{\Delta\nu}{c}\right)_w , \quad (1)$$

where α_w = water vapor absorption (km^{-1}),

ρ = water vapor density (gm^{-3}),

$\left(\frac{\Delta\nu}{c}\right)_w$ = line width (cm^{-1}),

$(\tilde{\nu},\tilde{\nu}_o)$ = wave number and resonant wave number (cm^{-1})

and T = absolute temperature (K)

The pressure, P (mb) and temperature dependence of the line width is

$$\left(\frac{\Delta\nu}{c}\right)_w = \left(\frac{P}{1013.25}\right)\left(\frac{318.0}{T}\right)^{.625} a(1+b\rho) \quad . \qquad (2)$$

Numerical values of the constants are

$C_1 = .0008312$

$C_2 = .01402$

$a = .08478$

$b = .00708$

$\tilde{\nu}_o = .7417\ cm^{-1}$.

The theory of microwave absorption by O_2 was given by Van Vleck [1947b] and has been qualitatively verified in the atmosphere by several measurements [Whitehurst, Copeland and Mitchell, 1957; Stafford and Tolbert, 1963; Barrett, Kuiper and Lenoir, 1966]. In this report, calculations of O_2 absorption are based on the Van Vleck theory with line width parameters determined by Carter, Mitchell, and Reber [1968]. The formulas used in the O_2 absorption calculations are given by

$$\alpha_{O_2} = C_3 \frac{P\nu^2}{T^3} \sum_{\substack{N=1 \\ odd}} \left(\mu^2_{N_+} f(\tilde{\nu}, \tilde{\nu}_{N_+}, \Delta\tilde{\nu}) + \mu^2_{N_-} f(\tilde{\nu}, \tilde{\nu}_{N_-}, \Delta\tilde{\nu}) + \mu^2_{N_O} f(\tilde{\nu}, 0, \Delta\tilde{\nu}) \right) e^{\frac{-B\,N(N+1)}{T}} , \qquad 3$$

where α_{O_2} = absorption coefficient in km^{-1},

$\tilde{\nu}_{N\pm}$ = resonant wave numbers of + and - transitions (cm^{-1}),

$$\mu^2_{N_+} = \frac{N(2N+3)}{N+1} ,$$

$$\mu^2_{N_-} = \frac{(N+1)(2N-1)}{N+1} ,$$

$$\mu^2_{N_O} = \frac{2(N^2+N+1)(2N+1)}{N(N+1)} ,$$

$$B = 2.068666 ,$$

and

$$C_3 = 13.693 .$$

If

$$\frac{\Delta\tilde{\nu}}{P} = \text{line width } (cm^{-1}/\text{ atm}) ,$$

then the form factors in (3) are given by

$$f(\tilde{\nu}, \tilde{\nu}_{N_\pm}, \Delta\tilde{\nu}) = \frac{\Delta\tilde{\nu}}{(\tilde{\nu} - \tilde{\nu}_{N_\pm})^2 + (\Delta\tilde{\nu})^2} + \frac{\Delta\tilde{\nu}}{(\tilde{\nu} + \tilde{\nu}_{N_\pm})^2 + (\Delta\tilde{\nu})^2} \quad . \qquad (4)$$

and

$$f(\tilde{\nu}, 0, \Delta\tilde{\nu}) = \frac{\Delta\tilde{\nu}}{\nu^2 + (\Delta\tilde{\nu})^2} \quad , \qquad (5)$$

where the line widths are assumed independent of N.

For the line broadening parameter, $\Delta\tilde{\nu}$, we use the empirical expression

$$\Delta\tilde{\nu} = g(h)\left(\frac{P}{P_o}\right)\left(\frac{T_o}{T}\right)^{X_5} \quad , \qquad (6)$$

where P_o is the sea level pressure, T_o = 300.0, h is the altitude above sea level, X_5 is the temperature dependence of the line width, and g(h) is an altitude factor defined in figure 4a.

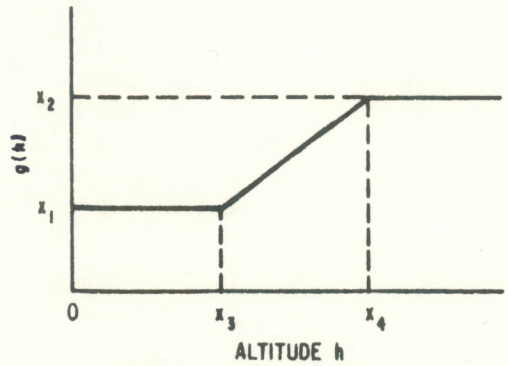

Figure 4a. Altitude factor for general line-broadning parameter. The line-broadning altitude parameters are X_1 = .0213 (cm^{-1}), X_2 = .0452 (cm^{-1}), X_3 = 8 (km), X_4 = 25 (km), X_5 = 1.0.

Calculations of gaseous microwave attenuation coefficients at sea level are shown in figure 4.

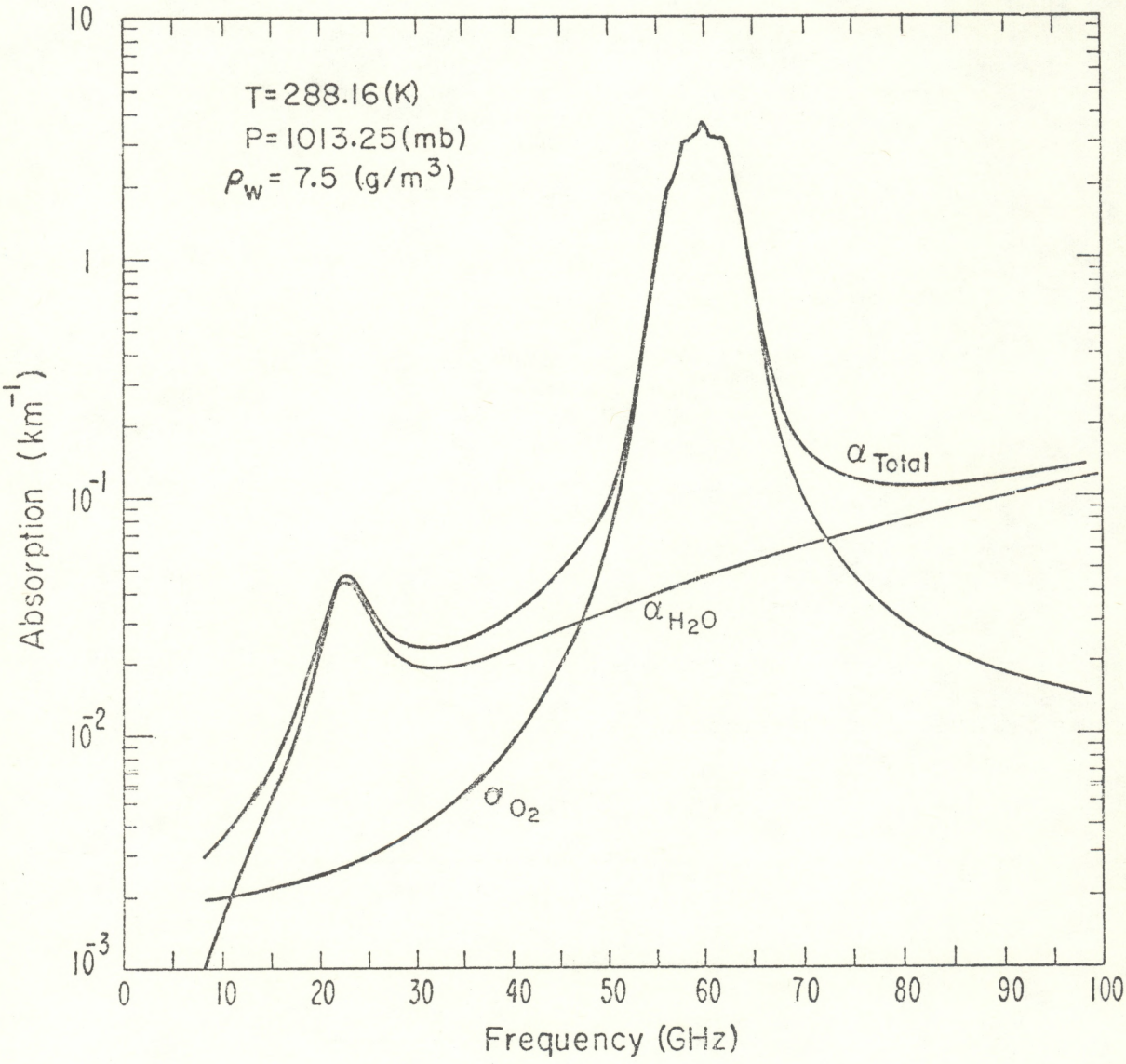

Figure 4. Gaseous microwave absorption.

4. ATTENUATION BY CLOUDS

The microwave absorption characteristics of water and ice spheres have been extensively studied by Deirmendjian [1963]. He shows that the extinction coefficient, for drop size distributions typical of non-precipitating clouds, can be expressed in terms of the liquid water content of the cloud particles, and is independent of the drop-size distribution. The scattering of energy is also small compared to the absorption so that the extinction and absorption coefficients are essentially equal. For frequencies considered in this report (<60 GHz), this approximation is valid for cloud particles of mode radius smaller than roughly 50 microns. Calculations of the accuracy of this approximation for a "gamma" distribution are given in Appendix A.

In the Rayleigh region, the extinction (or absorption) coefficient for spherical particles is given by

$$\alpha = \frac{1.885L}{\lambda} \; I\{-K\} \tag{7}$$

where

α = extinction coefficient (km^{-1})

λ = wavelength (cm)

L = liquid water content (g/m^3)

and

$$K = \frac{\varepsilon-1}{\varepsilon+2} \tag{8}$$

where ε = complex dielectric constant. The notation $I\{z\}$ means the imaginary part of the complex variable z.

The dielectric constant of water is given as a function of wavelength and temperature T(^{o}K), by Grant, et al. [1957] as

$$\varepsilon = \varepsilon_{\infty} + \frac{\varepsilon_{o} - \varepsilon_{\infty}}{1+\left(\frac{i\lambda_{s}}{\lambda}\right)^{1-\gamma}} \quad , \tag{9}$$

where

$$\varepsilon_{\infty} = 4.5 \quad ,$$

$$\varepsilon_{o} = \frac{32155.45}{T} - 29.62 \quad ,$$

$$\log_{10}\lambda_{s} = \frac{921.0935}{T} - 2.9014$$

and $$\gamma = .02 \quad .$$

The dielectric constant of ice is independent of frequency and temperature and is given by Deirmendjian [1963] as

$$\varepsilon = 3.1684 - 0.008544i \quad . \tag{10}$$

In this paper, two-component spherical drops have also been considered. Such a drop could describe a melting ice sphere. The Rayleigh extinction coefficient for a two-component sphere with an inner dielectric constant of ε_{1}, outer dielectric = ε_{2}, and ratio of

inner to total radius of q is again given by (7), but with K given by [Van de Hulst, 1957]

$$K(\varepsilon_1, \varepsilon_2, q) = \frac{\left[\varepsilon_2 - 1\right]\left[\varepsilon_1 + 2\varepsilon_2\right] + q^3\left[2\varepsilon_2 + 1\right]\left[\varepsilon_1 - \varepsilon_2\right]}{\left[\varepsilon_2 + 2\right]\left[\varepsilon_1 + 2\varepsilon_2\right] + q^3\left[2\varepsilon_2 - 2\right]\left[\varepsilon_1 - \varepsilon_2\right]} \quad . \qquad (11)$$

Calculations show the absorption from the two-component sphere can exceed that of an equivalent mass of either of its separate constituents. Figure 5 shows the calculated attenuation for ice, water, and a two-component mixture of ice and water with a radius ratio of 0.9.

For a given frequency, the two-component absorption exhibits a strong "resonant-like" behavior on the radius ratio q. As discussed in Appendix C, this dependence of the absorption on the relative geometry occurs because of a refractive effect in which the energy of the incident wave is concentrated in the lossy (water) medium. Figure 6 shows - I {K} vs. q at λ = 10 cm, and 0.5 cm. Note that all wavelengths show broad regions in which the "melting ice" sphere exhibits larger attenuation than a corresponding water sphere.

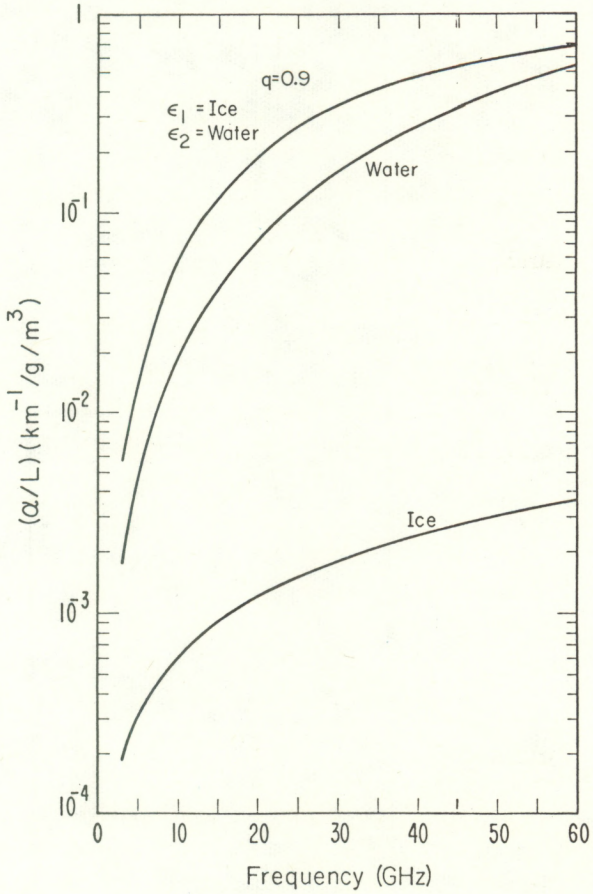

Figure 5. Calculated Rayleigh attenuation for water, ice and two-component ice-water spheres.

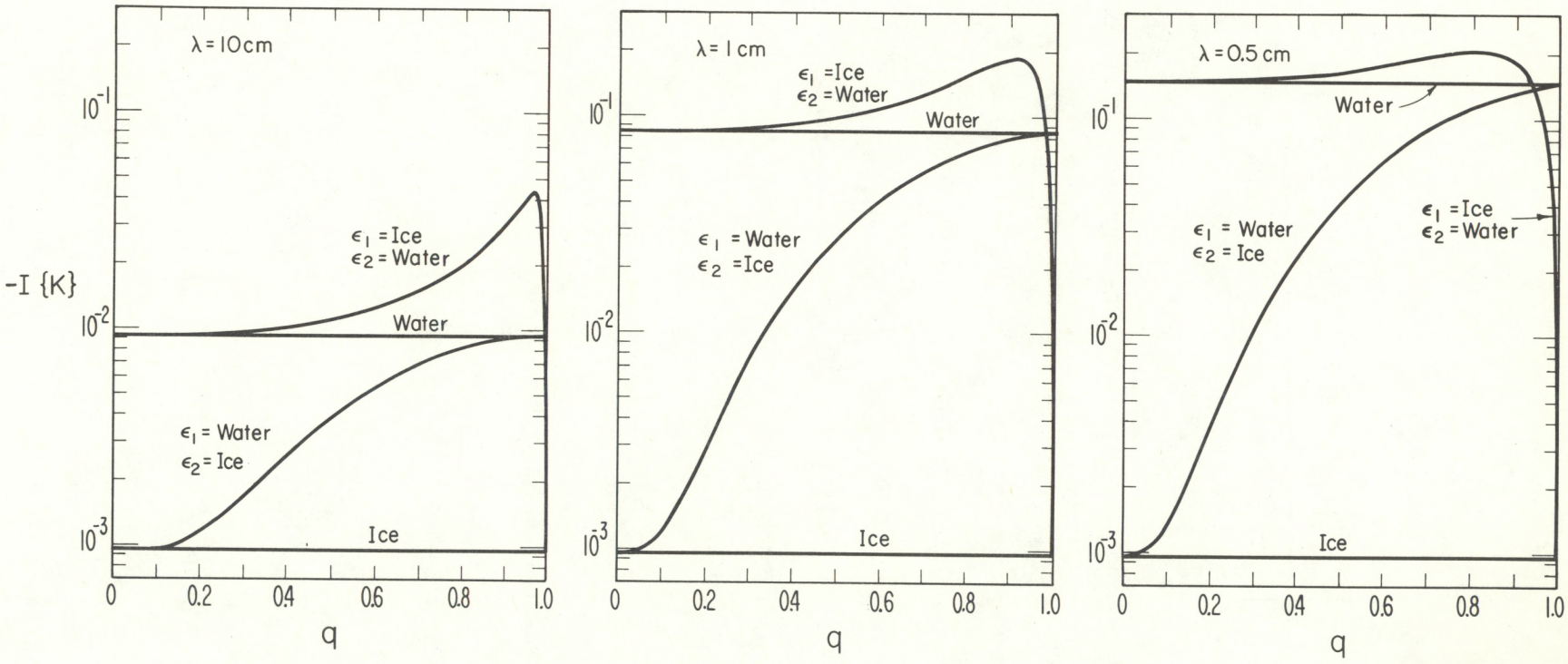

Figure 6. Dependence of attenuation of two-component spheres on q.

5. EMISSION CALCULATIONS

The microwave brightness temperature, $T_b^{\uparrow}$, observed from a satellite above a non-scattering atmosphere may be written

$$T_b^{\uparrow} = T_{b,A}^{\uparrow} + T_{b,s}^{\uparrow} + T_{b,R}^{\uparrow} \quad , \tag{12}$$

where

$$T_{b,A}^{\uparrow} = \int_0^{\infty} T\alpha \, e^{-\int_0^s \alpha ds} \, ds \quad , \tag{12a}$$

$$T_{b,s}^{\uparrow} = \varepsilon_s T_s e^{-\tau} \quad , \tag{12b}$$

$$T_{b,R}^{\uparrow} = (1 - \varepsilon_s) e^{-\tau} T_{b,D}^{\downarrow} \quad , \tag{12c}$$

$$T_{b,D}^{\downarrow} = \int_0^{\infty} T \alpha \, e^{-\int_0^{\ell} \alpha \, d\ell} \, d\ell \quad , \tag{12d}$$

and

$$\tau = \int_0^{\infty} \alpha \, ds \quad . \tag{12e}$$

In (12), $T_b\uparrow_{,A}$ represents the upward emission from the atmosphere, $T_b\uparrow$, s is the attenuated surface emission, $T_b{}^{\uparrow}{}_{,R}$ is the attenuated portion of reflected downward emission, $T_b{}^{\downarrow}{}_{,D}$, $d\ell$, and ds are increments of upward and downward arclength, τ is the total optical depth (opacity) of the atmosphere, and ε_s is the surface emissivity. For simplicity, we have assumed specular reflection in (12c).

The relative contribution of the various terms in (12) to the total brightness is a function of frequency, surface emissivity, and the vertical distribution of temperature and density parameters. Calculations of (12) at nadir for the clear U.S.A. 1962 Standard Atmosphere are shown in figure 7. The total emission depends strongly on surface emission for $\nu < 50$ GHz and, to a lesser extent, on the contribution of reflected downward emission. The emission calculations above 50 GHz were made at 53.5, 54.5, and 55.5 GHz.

Satellite measurements of upward thermal emission in the oxygen complex provide a potential method of determining vertical temperature distributions [Staelin, 1969]. The spatial resolution achievable in indirect temperature sensing is closely related to the shape and width of the weighting functions, $W(\nu, h)$,

$$W(\nu, h) = \alpha_\nu \, e^{-\int_0^h \alpha_\nu (h) \frac{ds}{dh} \, dh} \frac{ds}{dh} \quad . \tag{13}$$

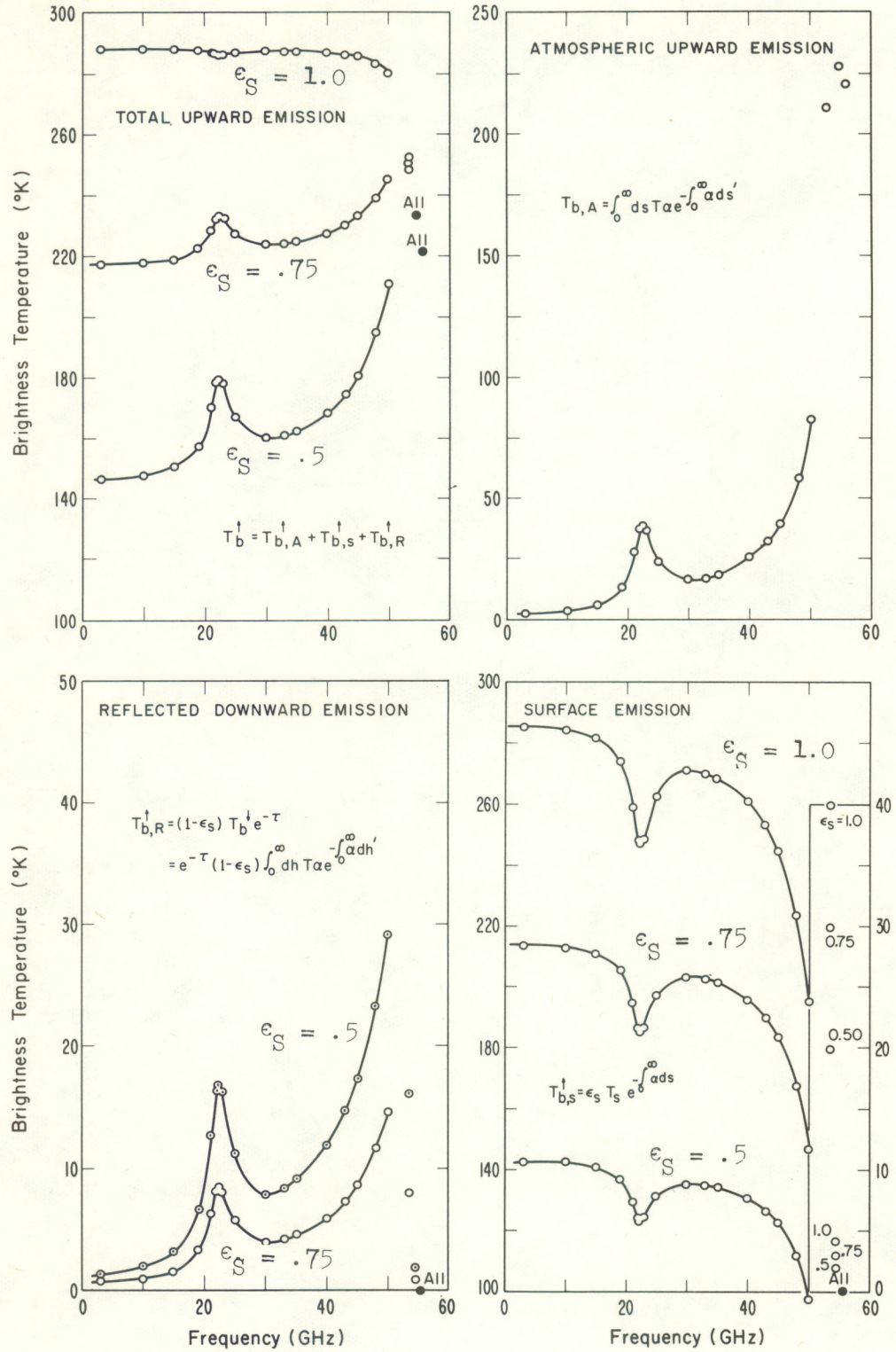

Figure 7. Nadir brightness temperatures for clear atmospheres.

Plots of nadir weighting functions $W(\nu, h)$ are shown in figure 8, for frequencies which cover the troposphere. The approximate widths of the weighting functions are between 10 to 13 km. From the set of functions shown in figure 8, the frequencies 53.5, 54.5, and 55.5 GHz were chosen for more extensive calculation. Weighting functions for these frequencies at nadir angles of 0.0, 60.0, 75.53, and 80.42 degrees are shown in figure 9. These angles give secant factors of 1, 2, 4, and 6, respectively.

The effect of clouds on weighting functions is an important consideration in indirect sensing of vertical temperature profiles. For the satellite problem, the general effect of an absorbing cloud layer is to uniformly decrease the weighting function below the cloud, to distort the function within the layer, and to leave it unchanged above the cloud. Calculations of weighting functions for a variety of cloud types are shown in figures 10 to 15 for the 1962 U. S. Standard, Tropical (15°N) and Subarctic (60°) Winter Cold atmospheres. These calculations assume pure water within the clouds and drop-size distributions that are within the Rayleigh region. Note that the 53.5 GHz functions are affected somewhat by all of the cloud models, and that strong thunderstorms affect all of the frequencies.

At frequencies removed from the oxygen complex, the effect of clouds on the total upward emission depends to a large extent on the surface emissivity. Calculations of nadir upward emission from water

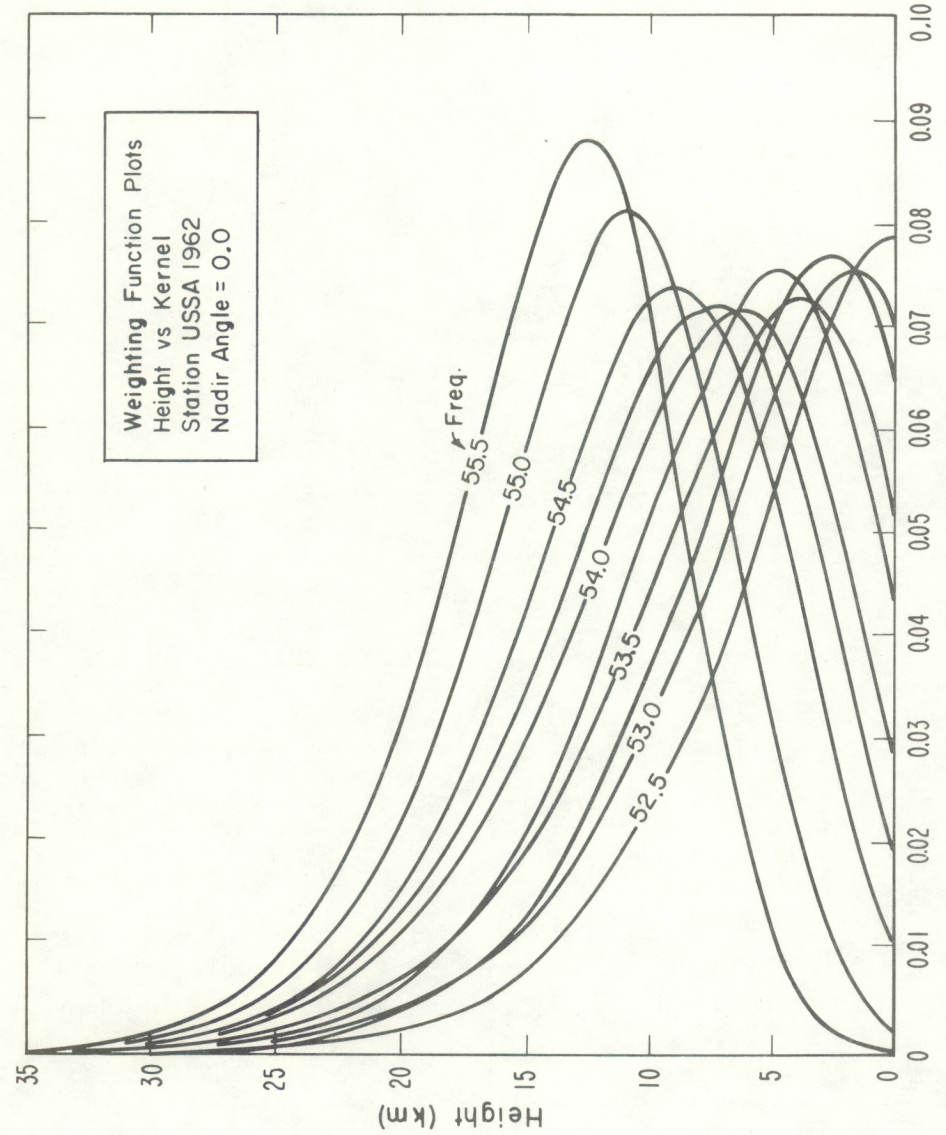

Figure 8. Nadir temperature weighting functions.

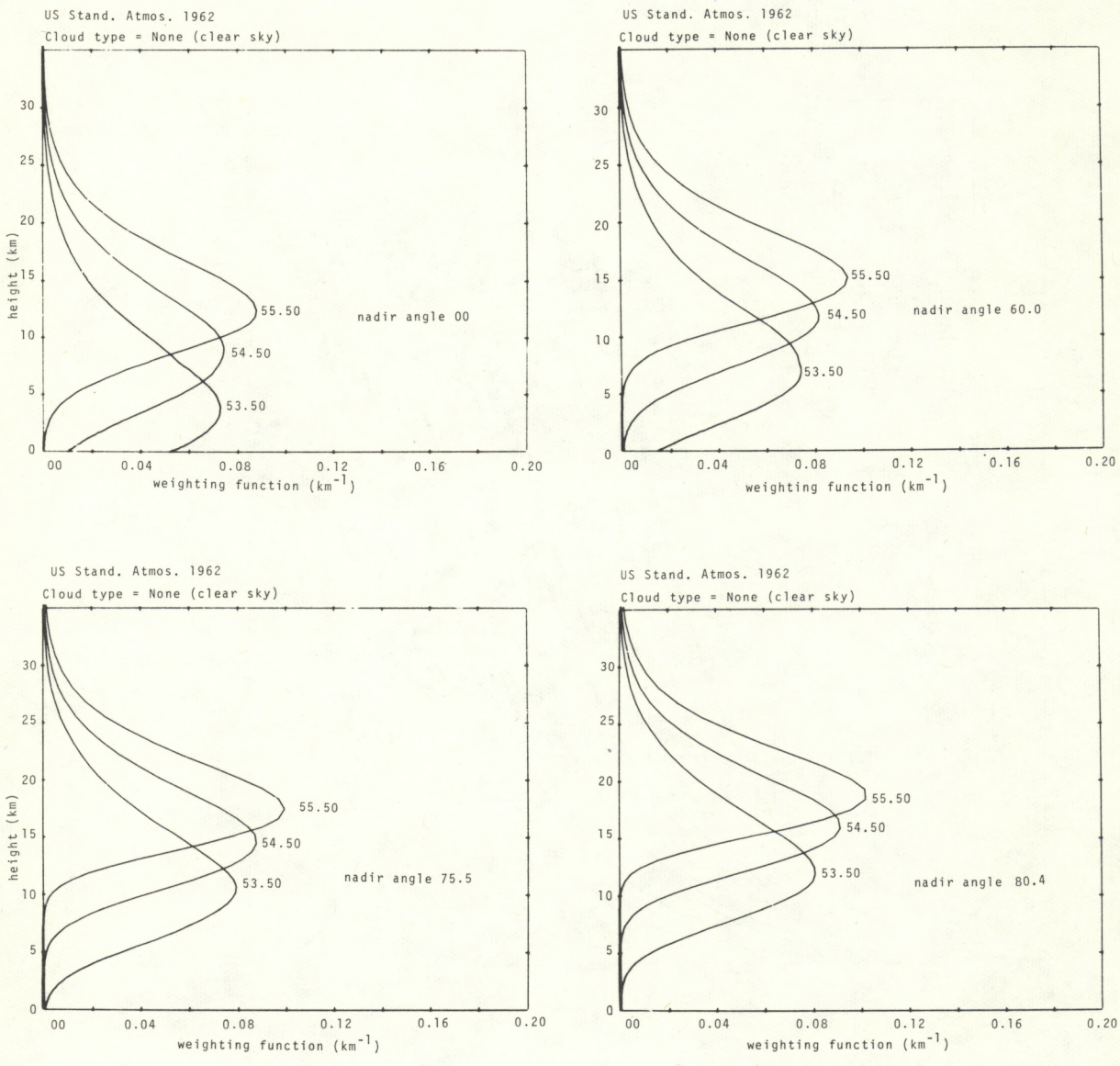

Figure 9. Temperature weighting functions for various nadir angles.

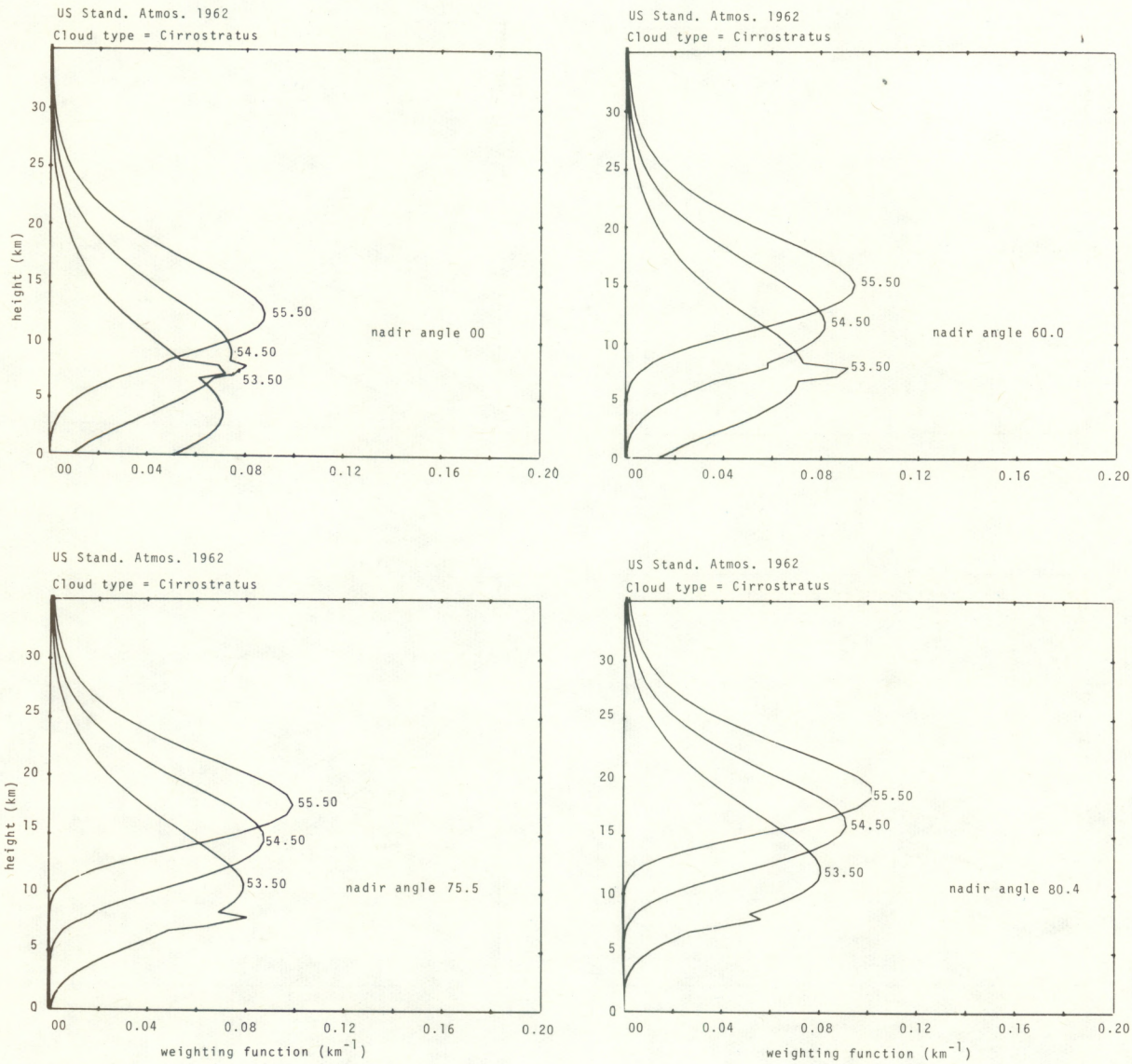

Figure 10. Effect of water clouds on temperature weighting functions.

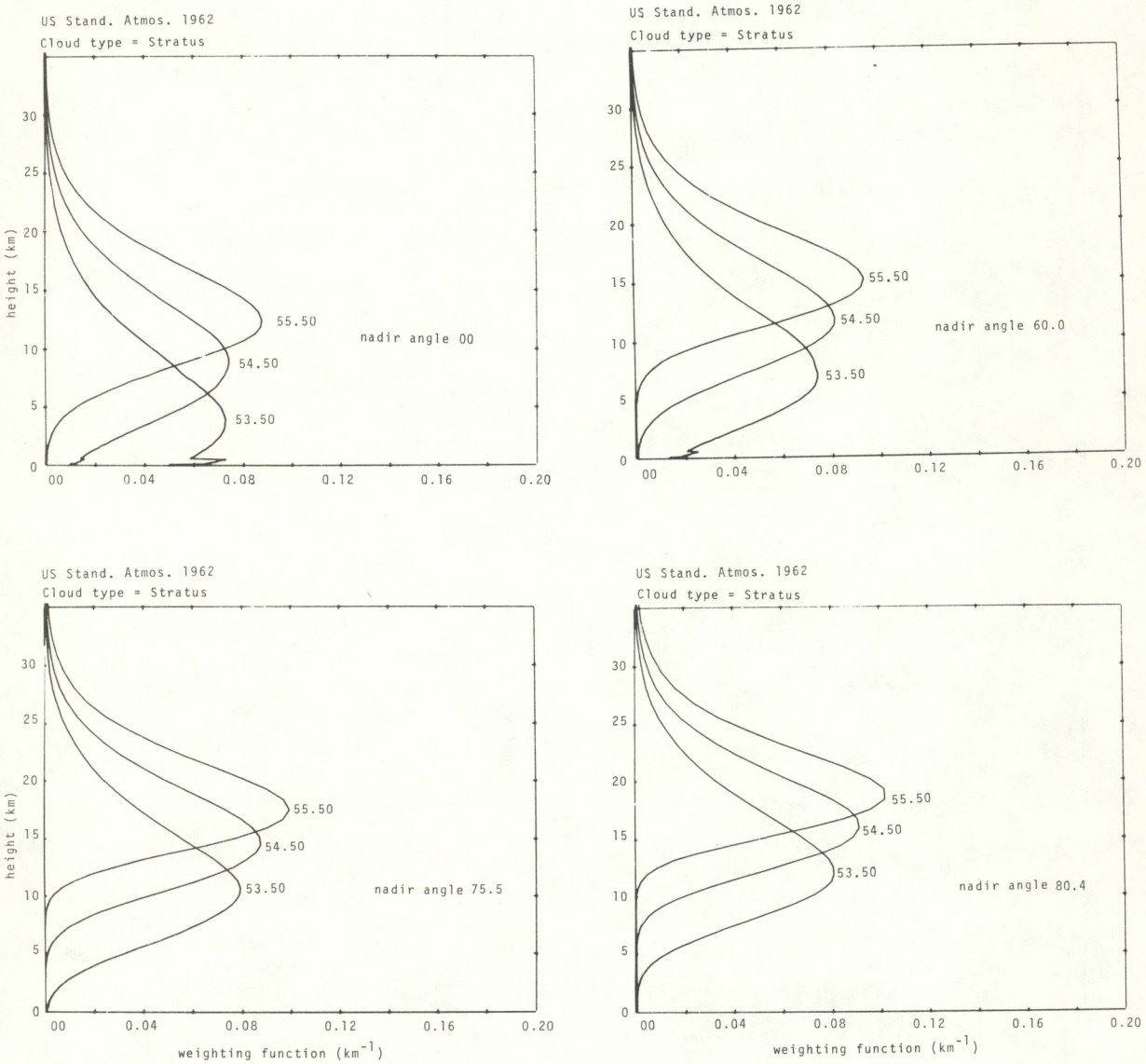

Figure 11. Effect of water clouds on temperature weighting functions.

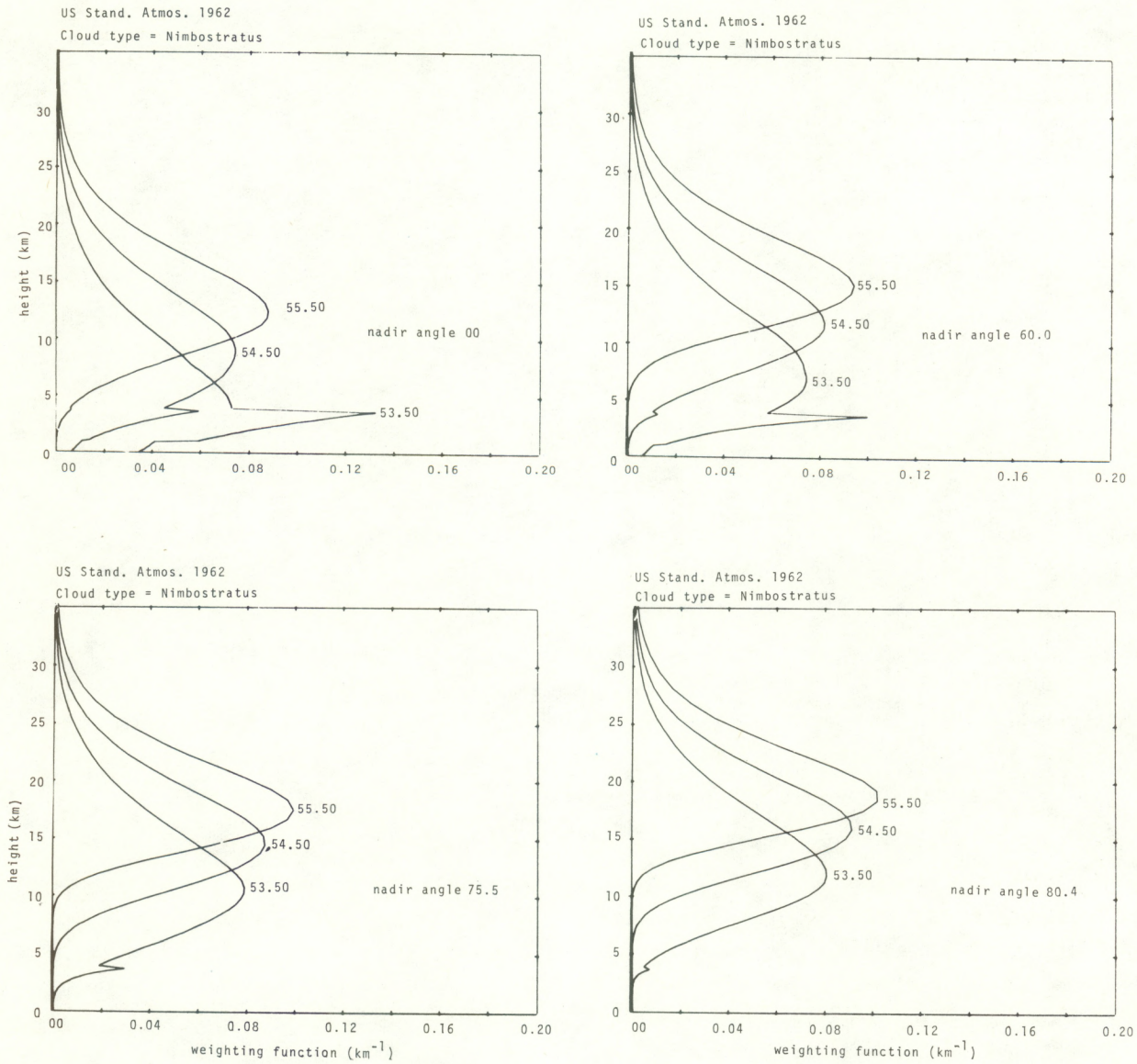

Figure 12. Effect of water clouds on temperature weighting functions.

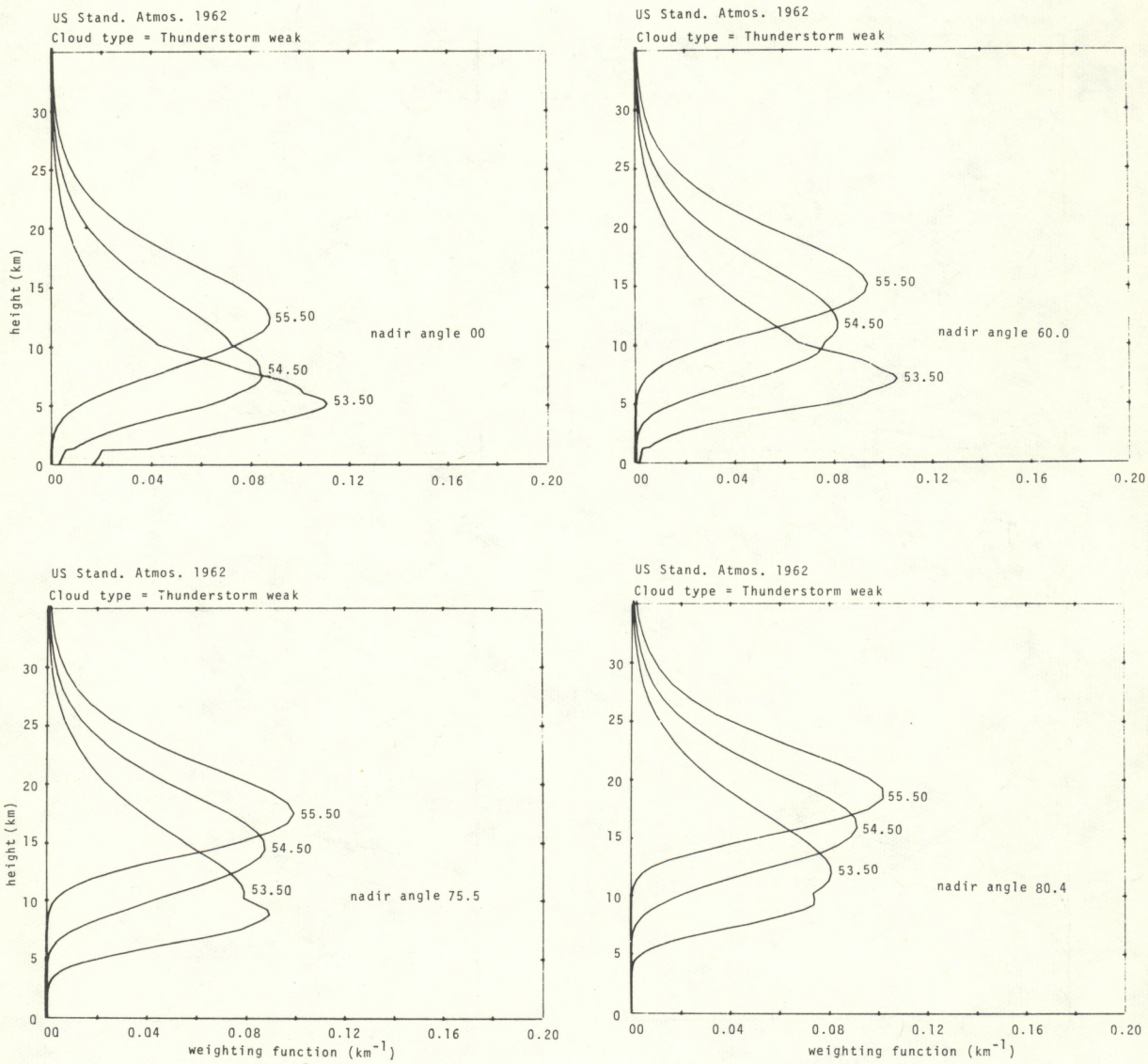

Figure 13. Effect of water clouds on temperature weighting functions.

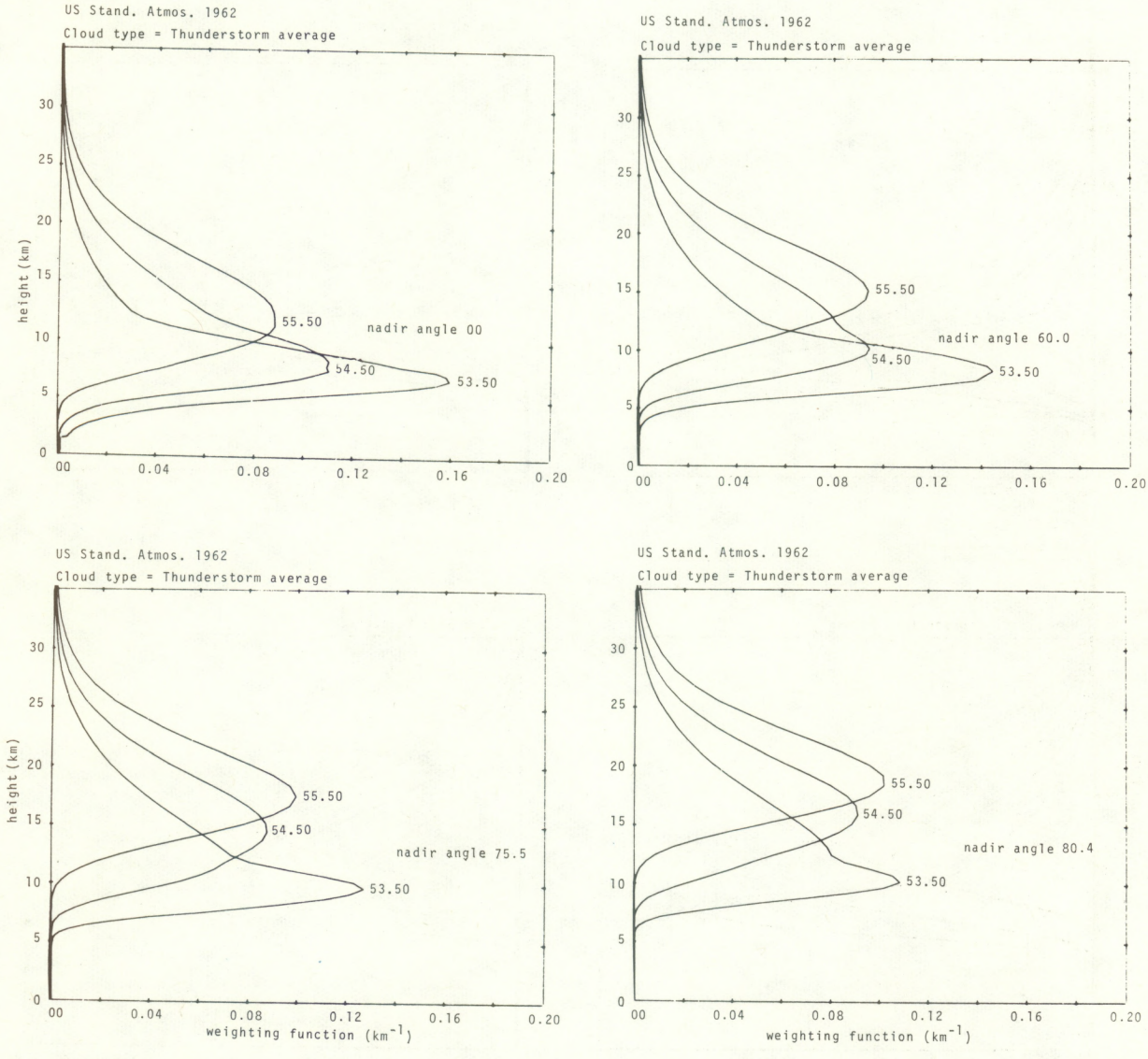

Figure 14. Effect of water clouds on temperature weighting functions.

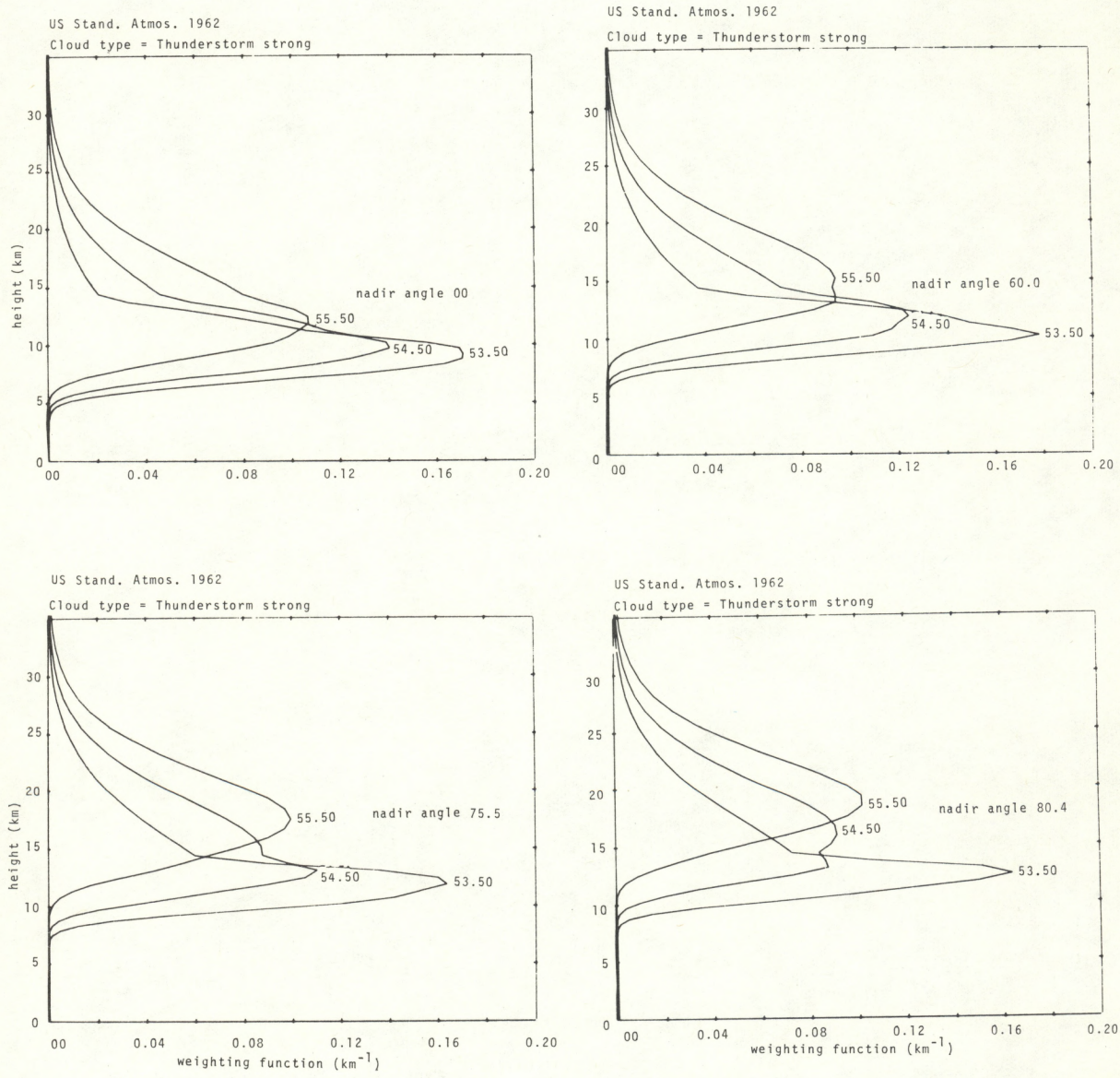

Figure 15. Effect of water clouds on temperature weighting functions.

clouds are shown in figures 16 to 18. Cloud calculations are at frequencies of 3, 10, 19, 22.235, 35, 53.5, 54.5, and 55.5 GHz. Note that thunderstorms strongly affect most frequencies. Also note that, for a given emissivity, the emission is not always a monotonic function of water content. For example, at ν = 35 GHz and ε_s = 0.5, the emission from the average thunderstorm exceeds that from the strong type by several degrees. This occurs here because the weighting function for the strong thunderstorm peaks at an altitude where the temperature is cold, while the warm emission from the ground is strongly attenuated. Corresponding opacity $\left(\int_0^\infty \alpha \, dh \right)$ calculations are shown in figure 19. The range in opacity is two orders of magnitude.

Calculations for ice and for two-component ice-water clouds were also performed for the 1962 standard atmosphere. The two-component model contained an inner sphere of ice with a radius of 0.9 of the total. Water clouds were assumed for T > 273.16 K. The vertical upward brightness temperatures are given in figure 20 for water to ice clouds, and in figure 21 for water to two-component clouds. Comparison of opacity calculations for water, water to ice, and water to two-component cloud distributions are shown in figure 22.

Two-component clouds effect weighting functions in a similar, but somewhat larger fashion than water clouds. However, because of the large difference in attenuation between water and ice, ice clouds affect the weighting functions less than water. This is illustrated

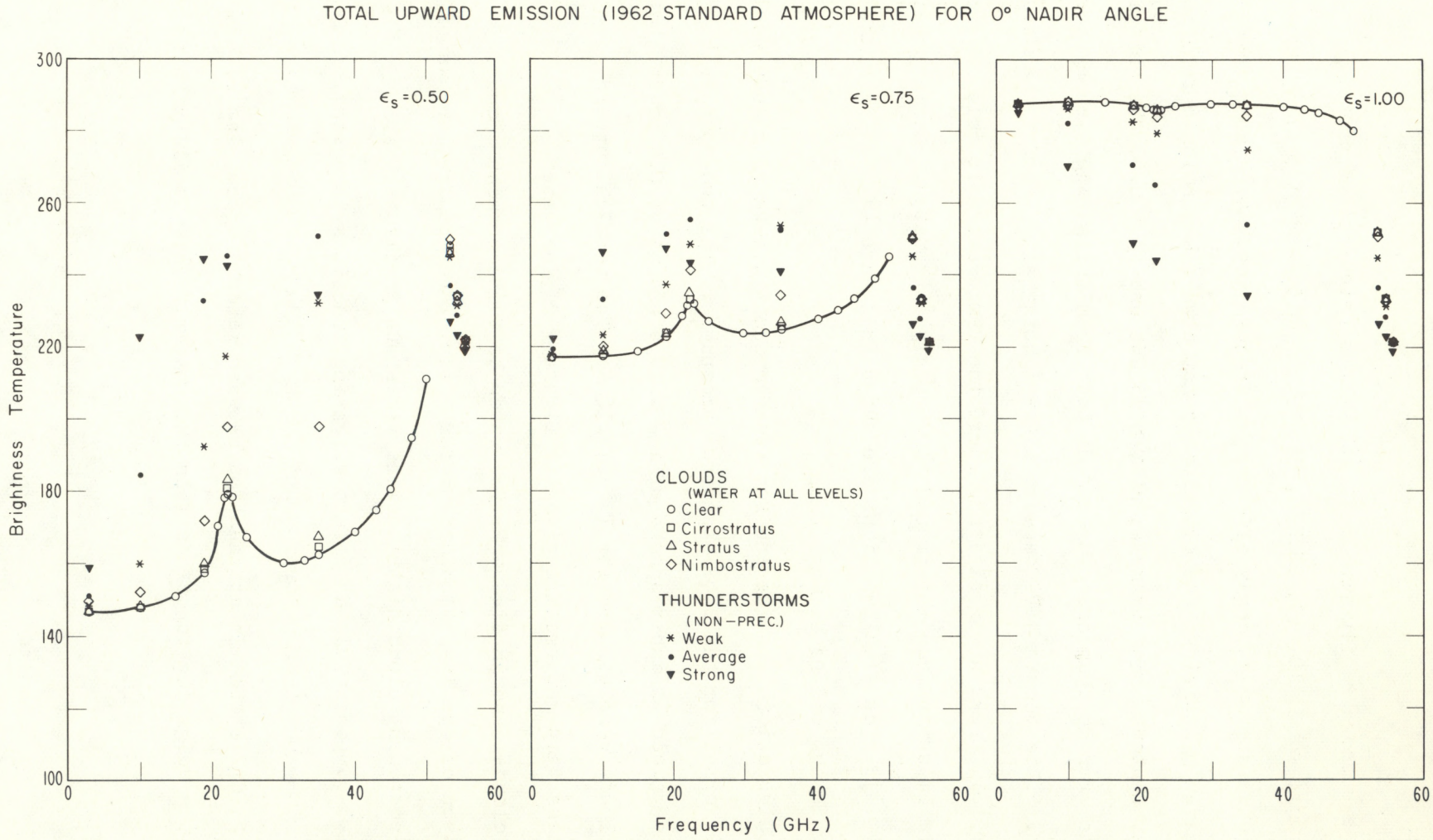

Figure 16. Nadir brightness for various cloud models.

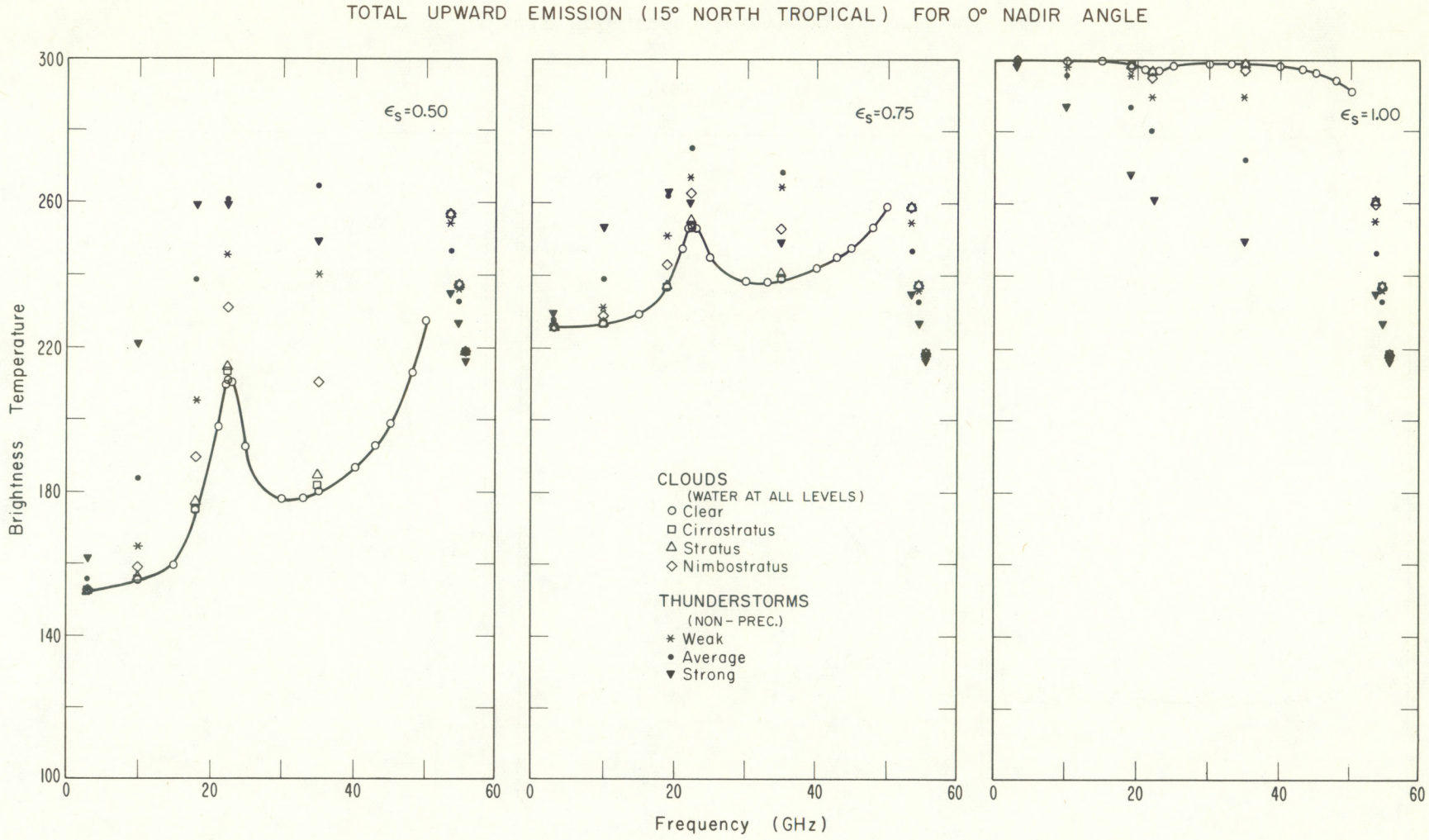

Figure 17. Nadir brightness for various cloud models.

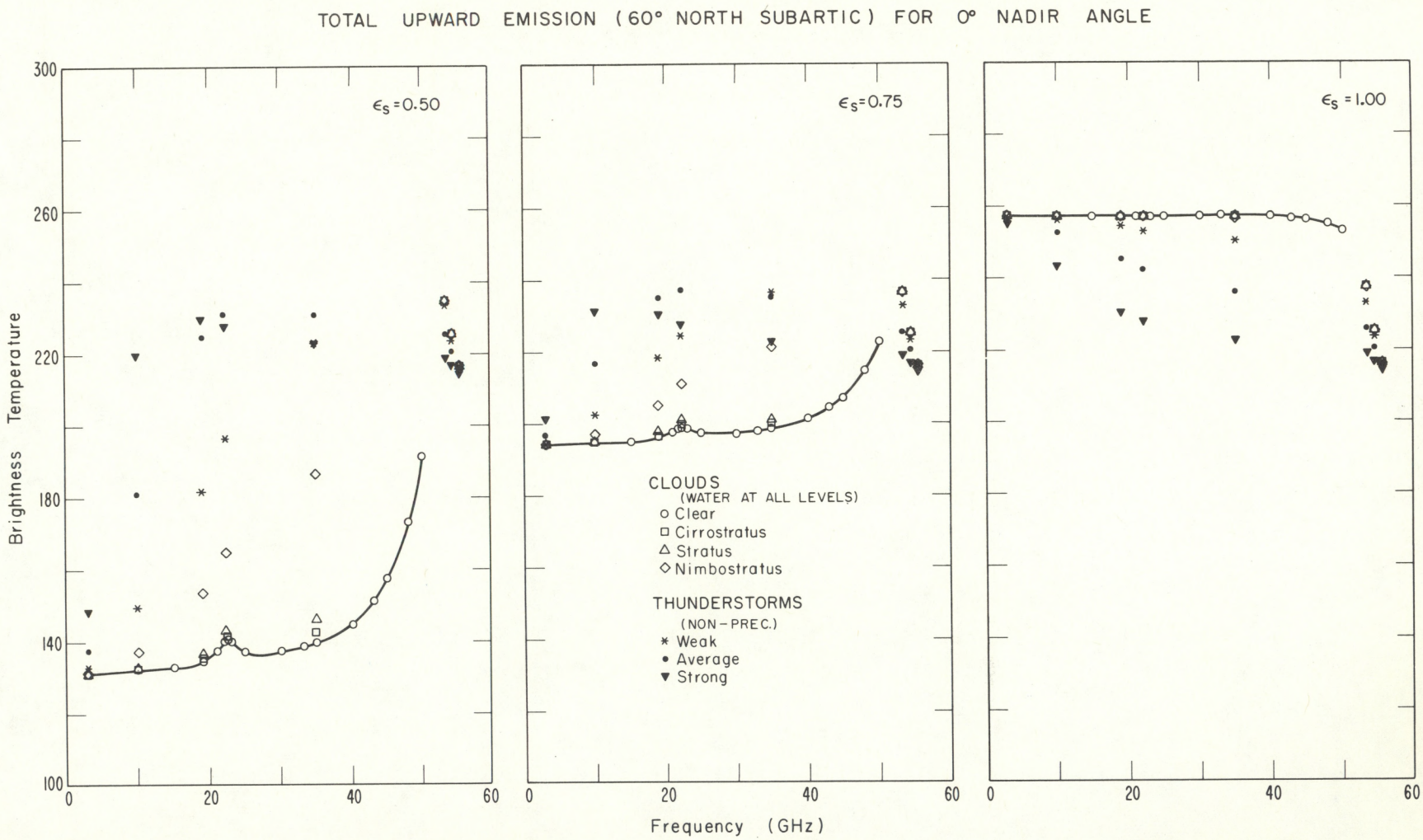

Figure 18. Nadir brightness for various cloud models.

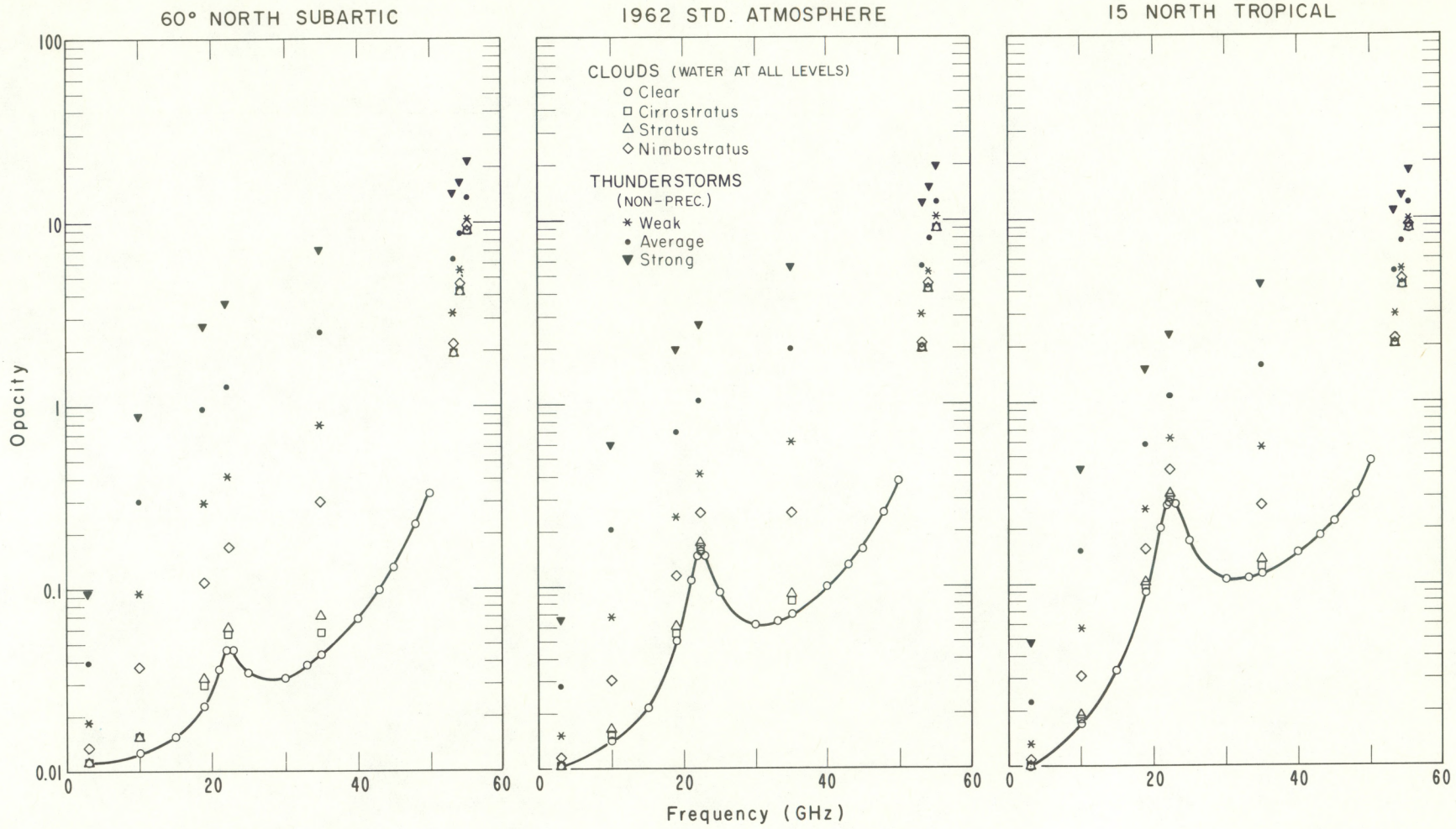

Figure 19. Opacity for various cloud models.

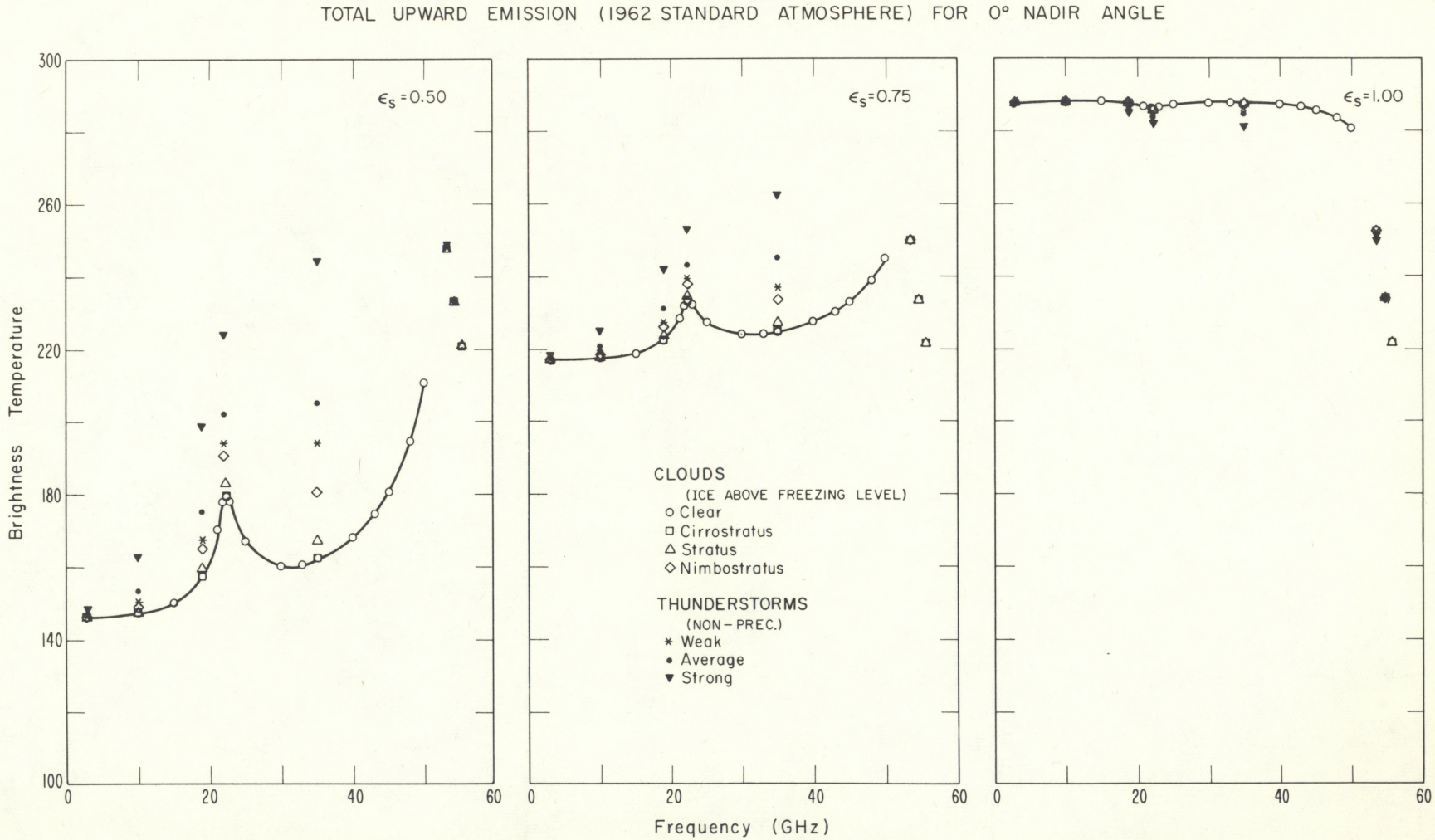

Figure 20. Nadir brightness for ice clouds above freezing level.

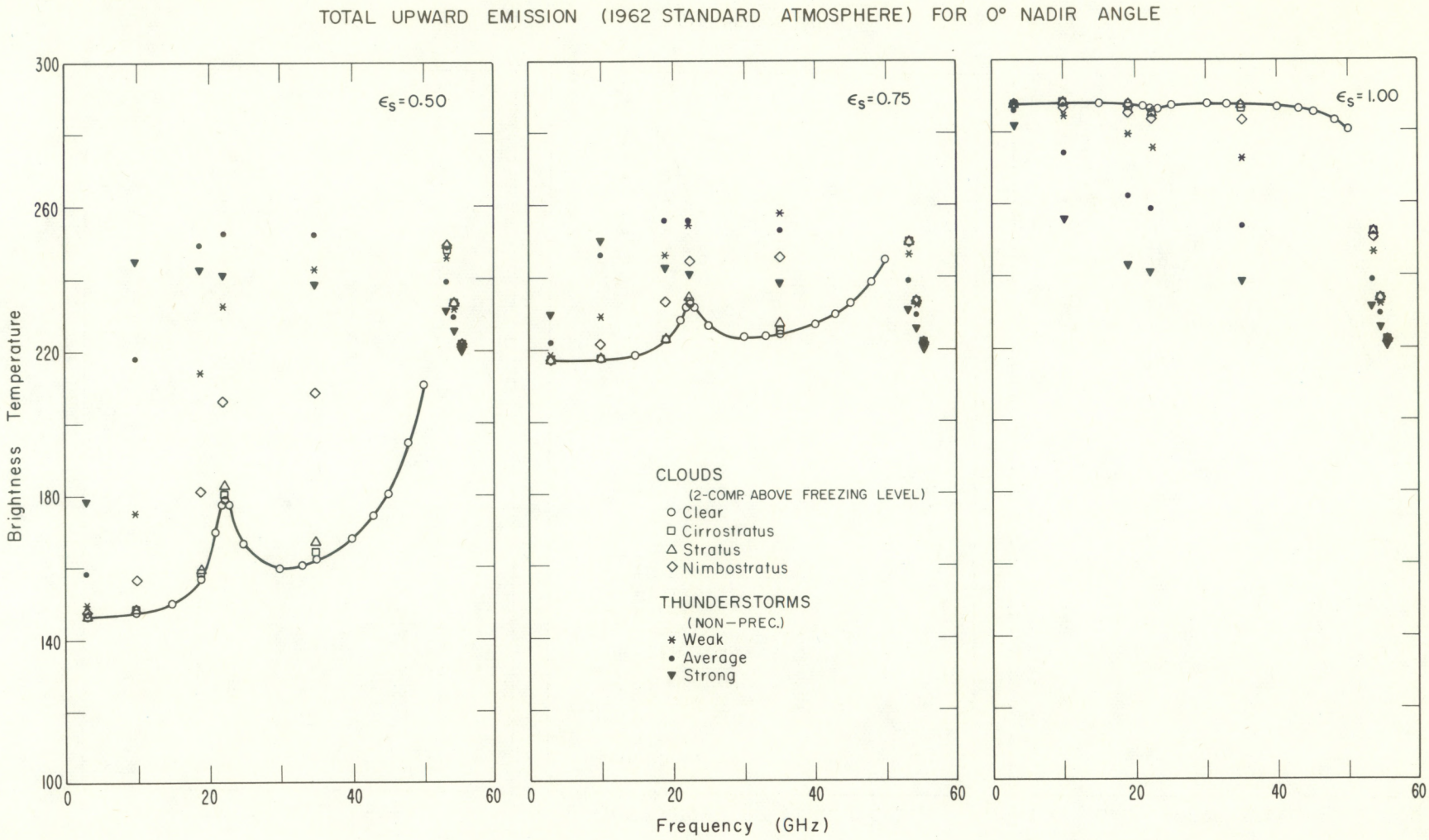

Figure 21. Nadir brightness for two-component clouds above freezing level.

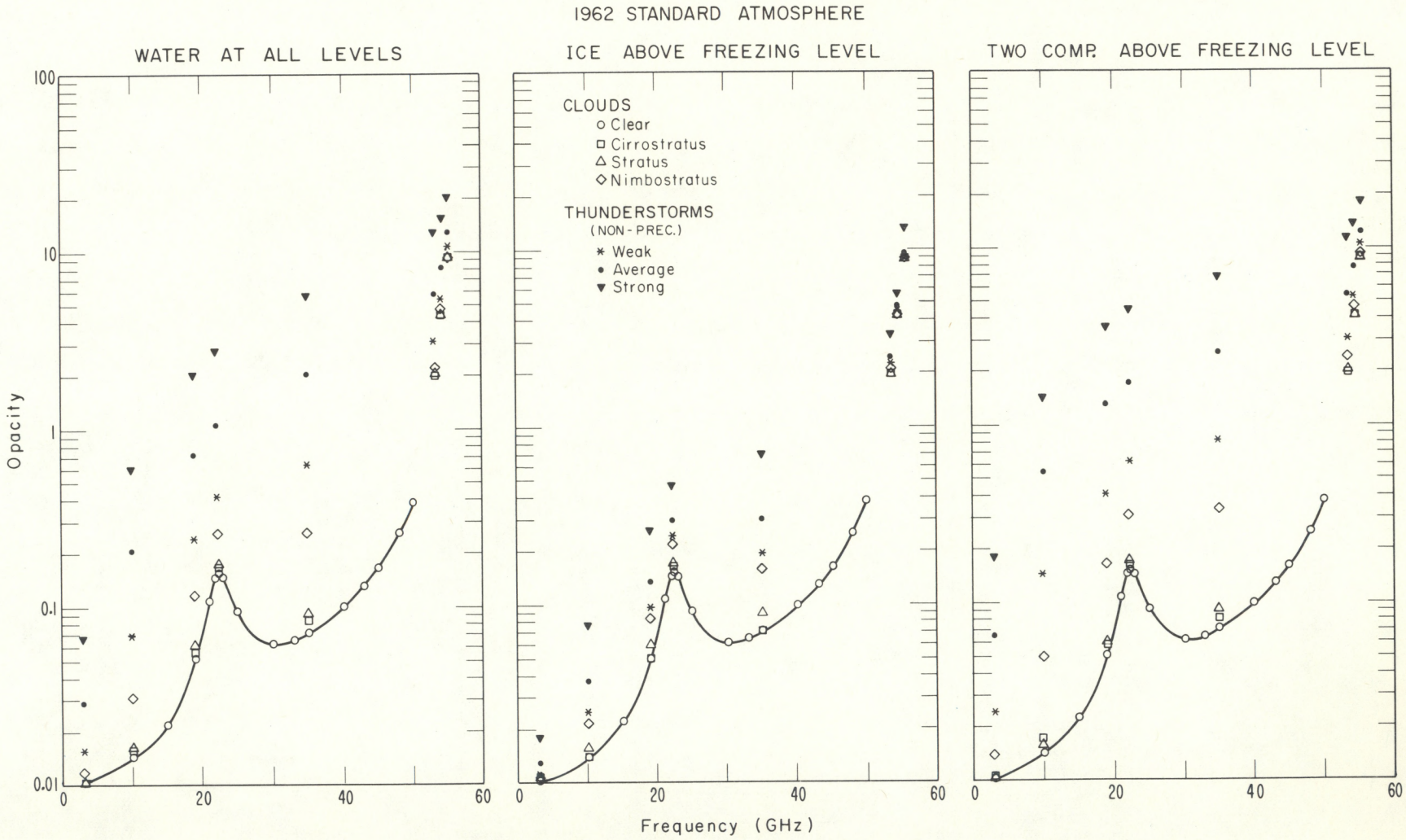

Figure 22. Opacity calculations for various ice-water clouds.

in figure 23, which shows weighting functions for the nimbostratus model. Approximately half of this cloud contains only ice. This figure should be compared with the corresponding figure 12 which shows calculations for water spheres.

The preceding calculations have shown the large variation in brightness that occurs for various cloud models. This variation depends on the cloud height, thickness, water content, and frequency. It has also been shown that for a given cloud geometry a large brightness variation can occur from varying amounts of water-ice phase. This is further illustrated in figure 24, which shows brightness calculations for the weak thunderstorm model with three assumed phase distributions.

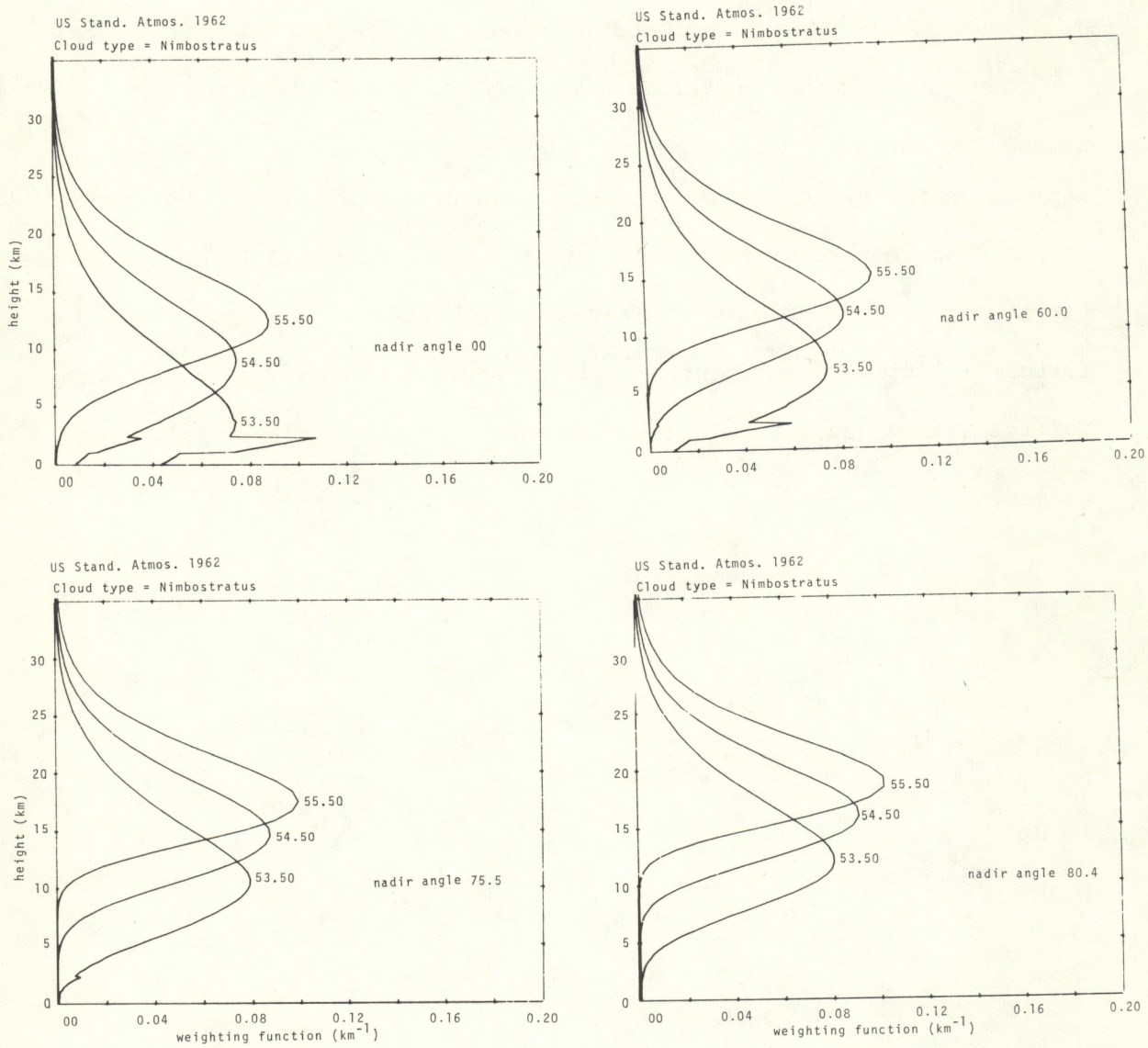

Figure 23. Temperature weighting function for ice clouds above freezing level.

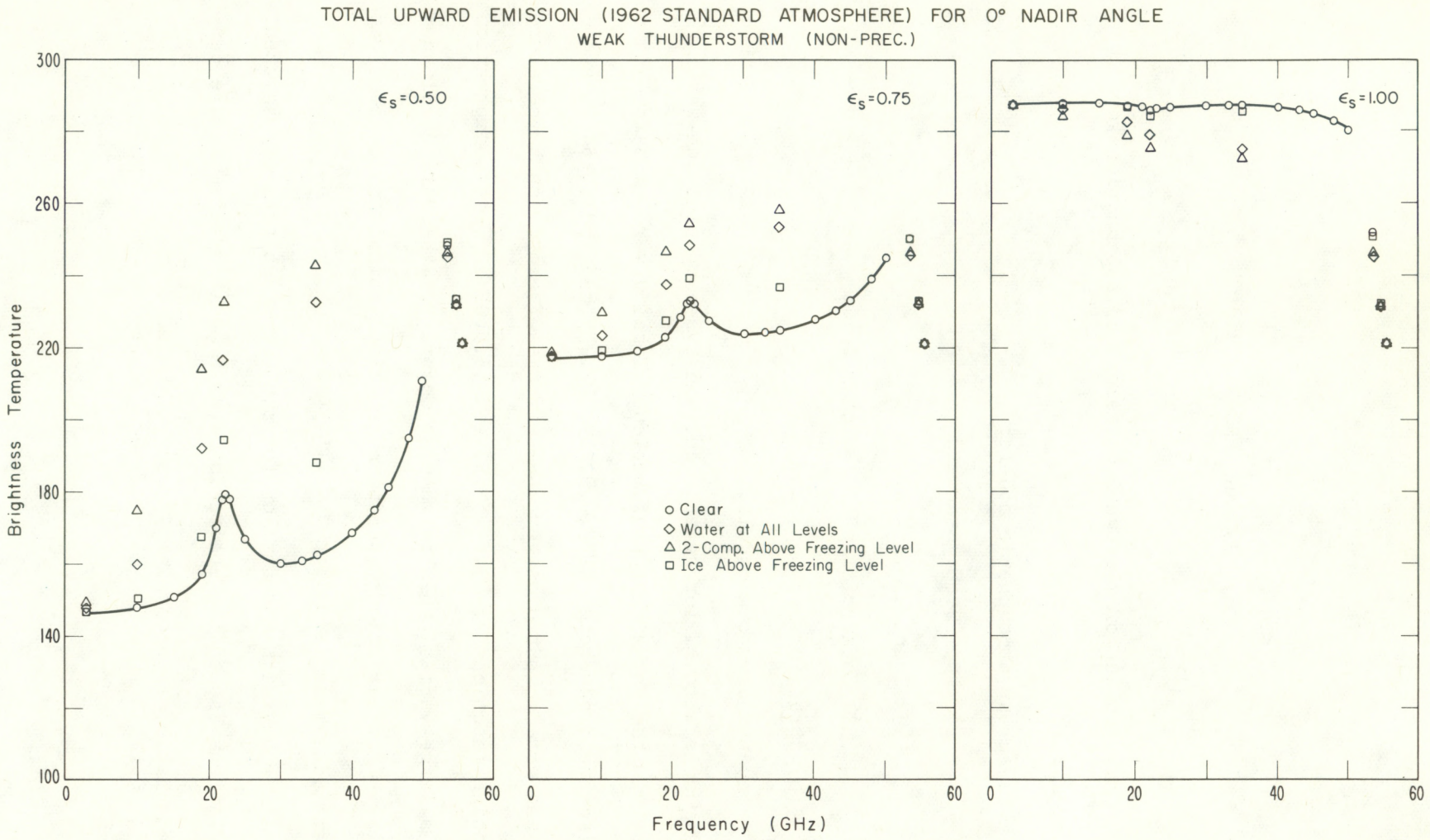

Figure 24. Nadir brightness calculations for various ice-water clouds.

6. SUMMARY AND DISCUSSION

Calculations of microwave emission and attenuation were presented for:

(a) clear atmospheric models:

(1) 1962 U. S. Standard

(2) Tropical (15° N)

(3) Subarctic (60° N) Winter Cold;

(b) stratiform clouds; and

(c) thunderstorm models.

Cloud models allowed for water, ice, and two-component ice-water spheres in the Rayleigh approximation. Total upward emission and opacity at discrete frequencies of 3, 10, 19, 22.235, 35, 53.5, 54.3, and 55.5 GHz were computed as were the effects of clouds on temperature weighting functions at 53.5, 54.5, and 55.5 GHz. These computations show a large variation in brightness occurs for the various cloud models. This variation depends on the cloud height, thickness, water content, ice-water fraction and frequency.

The Rayleigh attenuation for two-component spheres was studied. Calculations showed the absorption from a "melting-ice" sphere can exceed that of an equivalent amount of water or ice.

The theoretical limitations on the above spherical particle studies lie in two areas. First, for drop size distributions typical of rain and hail, Mie extinction coefficients must be integrated with the size distribution to provide adequate estimates of the extinction. Second, when the size distribution is such that scattering becomes important relative to absorption, this dependence must be taken into account in the transfer equation.

Future work in this area should include measurements of emission supplemented with direct measurements of cloud parameters, photographs of cloud structure from several viewing directions, and measurements of path length from cloud to observer. The measurements of attenuation at 15.25, 31.65, and 52.5 GHz, given in Appendix B, lacked all of the above information.

In this report, only the effect of clouds on the direct problem of radiative transfer has been considered. Their effect on the various inverse problems, and the extent to which they can be corrected is an important problem.

7. ACKNOWLEDGMENTS

The author gratefully acknowledges the superior computer programming and plotting assistance of Kelly Gregory and Michael D. Sauer. The work performed in this report was partially funded by the National Environmental Satellite Service.

8. REFERENCES

Barrett, A. H., J. W. Kuiper, and W. B. Lenoir (1966), Observations of microwave emission by molecular oxygen in the terrestrial atmosphere, J. Geophy. Res. 71, 4723-4734.

Becker, G. E., and S. H. Autler (1946), Water vapor absorption of electromagnetic radiation in the centimeter wavelength range, Phys. Rev. 70, 300-307.

Carter, C. J., R. L. Mitchell, and E. E. Reber (1968), Oxygen absorption measurements in the lower atmosphere, J. Geophy. Res. 73, 3121-3127.

Caton, W. M., W. J. Welch, and S. Silver (1967), Absorption and emission in the 8 mm region by ozone in the upper atmosphere, J. Geophy. Res. 72, 6137-6148.

Deirmendjian, D. (1963), Complete microwave scattering and extinction properties of polydispersed cloud and rain elements, Rand Corp. Report R-422-PR (USAF Contract No. AF-49(638)-700, Project Rand). Available: NTIS, Springfield, Va. 22151, AD426 139.

Falcone, V. (1966), Calculations of apparent sky temperature at millimeter wave lengths, Radio Sci. 1, (New Series) 1205-1209.

Feigel'son, E. M. (1966), Light and Heat Radiation in Stratus Clouds (Translated from Russian by Z. Lermans), Available: NTIS, Springfield, Va. 22151.

Grant, E. H., T. J. Buchanan, and H. F. Cook (1957), Dielectric behavior of water at microwave frequencies, J. Chem. Phys. 26, 156-161.

Handbook of Geophysics and Space Environments (1965), (Ed. Shea L. Valley), USAF Cambridge Research Laboratories, Cambridge, Mass.

Snider, J. B., and E. R. Westwater (1969), Atmospheric attenuation at 15, 31, and 53 GHz, ESSA Tech. Report ERL 156-WPL 11.

Staelin, D. H. (1966), Measurements and interpretation of the microwave spectrum of the terrestrial atmosphere near 1-centimeter wavelength, J. Geophy. Res. 71, 2875-2881.

Staelin, D. H. (1969), Passive remote sensing at microwave wavelengths, Proc. IEEE 57, 427-439.

Stafford, L. F., and C. W. Tolbert (1963), Shapes of oxygen absorption lines in the microwave frequency region, J. Geophy. Res. 68, 3431-3435.

Van de Hulst, H. C. (1957), Light Scattering by Small Particles, Wiley and Co., New York, New York.

Van Vleck, J. H. (1947a), The absorption of microwaves by oxygen, Phys. Rev. 71, 413-424.

Van Vleck, J. H. (1947b), Absorption of microwaves by water vapor, Phys. Rev. 71, 425-433.

Welch, W. J. (1968), A selective review of ground based passive microwave probing of the atmosphere, Atmospheric Exploration by Remote Probes 2, (Proc. of Scientific Meetings of Panel on Remote Atmospheric Probing, April 18-20 and May 16-17, 1968, National Academy of Sciences), 369-396.

Westwater, E. R. (1967), An analysis of the correction of range errors due to atmospheric refraction by microwave radiometric techniques, ESSA Technical Report IER 37-ITSA 37.

Whitehurst, R. N., J. Copeland, and F. M. Mitchell (1957), Solar radiation and atmospheric attenuation at 6-millimeter wavelength, J. App. Phys. 28, 295-298.

APPENDIX A

VALIDITY OF RAYLEIGH APPROXIMATION

The extinction coefficient, β_{ex}, describing a distribution of spherical scatterers and absorbers can be written [Kerr, 1951]

$$\beta_{ex} = \int_0^\infty \pi r^2 Q_{ex}(m, r)\, n(r)\, dr \quad , \tag{A1}$$

where r = particle radius,

$Q_{ex}(m, r)$ = extinction efficiency,

$n(r)\, dr$ = number of drops with radii between r and r + dr,

and m = complex refractive index

$= \nu - i\kappa$.

In the Rayleigh approximation, valid for $x = 2\pi r/\lambda << 1/\nu$,

$$Q_{ex} \simeq Q_{ab} = -4x \; I\left\{\frac{m^2 - 1}{m^2 + 2}\right\}$$

$$= -4x \; I\{K\} \quad , \tag{A2}$$

where Q_{ab} is the absorption efficiency.

Inserting (A2) into (A1) yields

$$\beta_{ex} = \frac{6\pi}{\lambda} \; I\{-K\} \; L \quad , \tag{A3}$$

where the liquid water content, L, is given by

$$L = \int_0^\infty \frac{4}{3} \pi r^3 \, n(r) \, dr \quad . \tag{A4}$$

Since the density of water is approximately 1 g/cm^3, L is frequently expressed in units of density. Equation (A3) expresses the important result that in the Rayleigh region the extinction coefficient is independent of the drop-size distribution and depends only on the liquid water content.

Penndorf [1962] gives an expansion of Q_{ex} (m, x) as

$$Q_{ex} = T_1 \, x + T_3 \, x^3 + T_4 \, x^4 \quad , \tag{A5}$$

where

$$T_i = \frac{24 \, \nu K}{Z_1} \quad , \tag{A5a}$$

$$T_3 = \frac{4}{3}\,\nu\kappa\left[\frac{1}{5} + \frac{5}{Z_2} + \frac{18}{5}\,\frac{7(\nu^2+\kappa^2)^2 + 4(\nu^2-\kappa^2-5)}{Z_1^2}\right], \qquad \text{(A5b)}$$

$$T_4 = \frac{8}{3}\,\frac{\left[(\nu^2+\kappa^2)^2 + (\nu^2-\kappa^2-2)\right]^2 - 36\,\nu^2\kappa^2}{Z_1^2}, \qquad \text{(A5c)}$$

$$Z_1 = (\nu^2+\kappa^2)^2 + 4(\nu^2-\kappa^2) + 4, \qquad \text{(A5d)}$$

and

$$Z_2 = 4(\nu^2+\kappa^2)^2 + 12(\nu^2-\kappa^2) + 9. \qquad \text{(A5e)}$$

The departure of the extinction from its Rayleigh approximation can be examined by integrating (A5) with physically realistic drop-size distributions. As discussed by Deirmendjian [1963], a particularly good analytic drop-size distribution is the "gamma" distribution

$$n(r) = ar^{\gamma} e^{-br^{\delta}}, \qquad \text{(A6)}$$

where

$$a = \frac{\delta N b^{\frac{\gamma+1}{\delta}}}{\Gamma\left(\frac{\gamma+1}{\delta}\right)} \quad , \tag{A6a}$$

and

$$b = \gamma \delta^{-1} r_c^{-\delta} \quad . \tag{A6b}$$

Above, N is the total number of drops per unit volume and r_c is the mode radius; i.e., the radius at which n(r) is a maximum. By adjusting the positive constants γ, b, and δ, (A6) can be made to fit many observed drop soze distributions. For the cloud calculations presented here, we choose N = 100 particles/cm^3, $\gamma = 6$, $\delta = 1$, and allow r_c to range between 4 to 100 μ. The calculations for λ = 10 cm, 1 cm, and 0.5 cm are shown in Table A-1 for ice spheres and in Table A-2 for water spheres. The maximum departure from the Rayleigh approximation is around 4.5 percent for $r_c \leq 30$ μ, but the error at $r_c = 100$ μ is serious at $\lambda = 0.5$ cm. Deirmendjian [1963] has shown that the full Mie equations must be used to calculate extinction for distributions describing rain, even for $r_c = 50$ μ.

Table A-1. Departure from Rayleigh Approximation to Extinction Coefficient ($km^{-1}/g/m^3$) for Ice Spheres.

	λ (cm)		
$r_c(\mu)$	10	1	0.5
4	1.80872×10^{-4}	1.80877×10^{-3}	3.61801×10^{-3}
5	1.80872 "	1.80880 "	3.61847 "
10	1.80872 "	1.80924 "	3.62428 "
15	1.80872 "	1.81027 "	3.63889 "
20	1.80873 "	1.81214 "	3.66631 "
30	1.80874 "	1.81944 "	3.77568 "
40	1.80877 "	1.83315 "	3.98461 "
50	1.80880 "	1.85528 "	4.32527 "
100	1.80924 "	2.16263 "	9.13120 "
Rayleigh	1.80872×10^{-4}	1.80872×10^{-3}	3.61743×10^{-3}

Table A-2. Departure from Rayleigh Approximation to Extinction Coefficient ($km^{-1}/g/m^3$) for Water Spheres.

	λ (cm)		
$r_c(\mu)$	10	1	0.5
4	1.75940×10^{-3}	1.59342×10^{-1}	5.55788×10^{-1}
5	1.75942 "	1.59362 "	5.55898 "
10	1.75955 "	1.59527 "	5.56822 "
15	1.75977 "	1.59804 "	5.58386 "
20	1.76008 "	1.60195 "	5.60605 "
30	1.76096 "	1.61319 "	5.67088 "
40	1.76220 "	1.62911 "	5.76413 "
50	1.76379 "	1.64981 "	5.88727 "
100	1.77712 "	1.82849 "	7.00179 "
Rayleigh	1.75937×10^{-3}	1.59307×10^{-1}	5.55593×10^{-1}

REFERENCES

Deirmendjian, D. (1963), Complete microwave scattering and extinction properties of polydispersed cloud and rain elements, Rand Corp. Report R-422-PR (USAF Contract No. AF-49(638)-700, Project Rand). Available: NTIS, Springfield, Va. 22151, AD426 139.

Kerr, D. E. (1951), Propagation of Short Radio Waves 13, (M.I.T. Rad. Lab. Ser.) McGraw-Hill, New York, New York.

Penndorf, R. B. (1962), Scattering and extinction coefficients for small absorbing and nonabsorbing aerosols, J. Opt. Soc. Am. 52, 896-904.

APPENDIX B

ATTENUATION BY CLOUDS AT 15, 31, and 53 GHz

J. B. Snider

1. INTRODUCTION

During July and August 1968, radiometric measurements of atmospheric attenuation were performed at Upolu Point, Hawaii, for a two-week period. Attenuation was measured in two ways: in the first, attenuation was measured directly using the sun as a signal source; in the second, atmospheric absorption was determined indirectly from emission measurements. Data were acquired at frequencies of 15.25, 31.65, and 52.50 GHz. A detailed description of the experiment and initial results are given in Snider and Westwater [1969]. The present work further examines these data to determine an order of magnitude estimate of the attenuation caused by clouds during the brief measurement period.

2. SOLAR MEASUREMENTS

Snider and Westwater [1969] discuss their direct attenuation measurements for the clear atmosphere as given by a secant law analysis. In their study, data where clouds are present are necessarily not considered to insure validity of the secant law. In the present work, all data are used and by assuming a constant solar brightness temperature,

each passage of the sun through the antenna beam yields an attenuation measurement.

The experimental procedure was to record solar emission as a function of zenith angle; this was accomplished by presetting the antenna elevation and azimuth angles prior to passage of the sun through the antenna beam. At 15 and 31 GHz, data were recorded at 10-minute intervals during the 1 1/2 hours after sunrise and before sunset. Solar data were not recorded at intermediate times because of the small rate of change of attenuation with zenith angle. However, at 52.50 GHz, data were recorded at 10-minute intervals throughout the day except for those periods when the zenith angle exceeded about 70°; this limitation was necessary because of the extremely high attenuation at the large zenith angles. Solar measurements were also interrupted at certain intervals to record atmospheric emission versus antenna elevation angle.

The attenuation observed during each drift curve is given by the ratio of the antenna temperature at the peak of the solar passage to the peak antenna temperature that would be produced by the sun in the absence of the earth's atmosphere. In Snider and Westwater [1969] it is shown that the latter antenna temperature can be determined from the variation of solar antenna temperature with zenith angle. For the results presented here, the solar brightness temperature without an atmosphere was determined for each frequency using only the clear sky solar data; it is also assumed that the solar brightness

temperature remained constant during the measurement period.

The results are presented in terms of the attenuation relative to gaseous absorption. Because of the relatively few numbers of data points at a given elevation angle and the fact that spatial information on the clouds does not exist, the data at all elevation angles have been combined. At 15 and 31 GHz, the elevation angles range from 5° to 60°; at 52.50 GHz, the variation in elevation is from 20° to 87°.

The various cloud types in the radiometer antenna beams were classified and recorded by the equipment operators. For the purposes of this report, the cloud data are classified in three main categories as follows: clear; light cloud cover, e.g., cirrus, altocumulus; and heavy cloud cover, e.g., cumulus or overcast. The three classifications are designated sky codes: 1, 2, and 3, respectively. Table B-1 lists the number of events and average attenuation relative to gaseous absorption by the clear atmosphere for the various frequencies and cloud categories. The values of average attenuation that depart slightly from zero gaseous absorption in the clear sky case are partly a result of the technique used to determine the solar brightness temperature in the absence of an atmosphere. Since the latter brightness temperatures were determined from a least squares fit to the individual drift curves, a small variation from the gaseous value is to be expected.

Table B-1. Summary of Average Attenuation for Three Cloud Categories.

Sky Code	Relative Attenuation (dB)	Number of Samples
	15.25 GHZ	
1	+0.009	50
2	-0.002	156
3	+0.033	28
	31.65 GHz	
1	+0.057	50
2	+0.111	156
3	+0.336	28
	52.50 GHz	
1	+0.081	171
2	+0.026	259
3	+0.623	87

Cumulative distributions of the attenuation relative to the clear air value are shown in figure B-1. Figure B-2 presents the distributions at all three frequencies when all cloud conditions are combined. When comparing the data, it should be remembered that while the 15 and 31 GHz data were recorded simultaneously, the 52.50 GHz data recording periods do not coincide with the lower frequency data.

3. ATMOSPHERIC EMISSION MEASUREMENTS

During times when solar data were not being recorded, atmospheric brightness temperature at the lower frequencies was recorded either at a fixed elevation angle of 7.5° on a semi-continuous basis, or periodically as a function of elevation angle. As discussed in Snider and Westwater [1969], emission measurements may yield absorption data if the kinetic temperature distribution of the atmospheric absorbers is known. However, for the case of the atmosphere, a mean radiating temperature is usually assumed and the absorption is calculated from

$$L_a = \frac{T_{mr}}{T_{mr} - T_{bm}} \qquad \text{(B-1)}$$

where L_a is the atmospheric loss factor, T_{bm} is the measured brightness temperature, and T_{mr} is the mean radiating temperature of the atmospheric absorbers.

For the present analysis, the brightness temperatures recorded at 7.5° elevation angle have been converted to absorption data by assuming a mean radiating temperature of 283 K for both clouds and the clear atmosphere. This value was selected after examination of the integrated absorption and brightness temperatures calculated from radiosonde data recorded at Upolu Point during the course of the measurements. At an elevation angle of 7.5°, the calculated mean radiating temperature is 281.5 K and 283.1 K at 15 and 31 GHz, respectively. On this basis, 283 K was estimated to be a reasonable value for T_{mr}.

Figure B-3 shows the cumulative distribution of the absorption derived from the emission measurements - the results are normalized to clear air absorption. The emission data base consists of approximately 174 total hours recording time - the data were read at 2-minute intervals. The values of attenuation occurring for 1 percent and less of the total samples are due to rain squalls; the remaining data are for clouds or clear air.

4. CONCLUSION

The chief purpose of this appendix has been to indicate the general magnitude of attenuation caused by clouds at frequencies near 15, 31, and 53 GHz during a brief measurement period on the Island of Hawaii. The approach has of necessity been semi-empirical due to the lack of quantitative information, e.g., liquid water content, spatial

extent, about the clouds. However, the results clearly indicate the contaminating properties of clouds that must be considered when using microwaves as a remote sensing tool.

5. REFERENCE

Snider, J. B., and E. R. Westwater (1969), Atmospheric attenuation at 15, 31, and 53 GHz, ESSA Technical Report ERL 156-WPL 11

FIGURE CAPTIONS - Appendix B

Figure B-1. Cumulative distribution of attenuation relative to clear air.

Figure B-2. Cumulative distribution of attenuation relative to clear air.

Figure B-3. Cumulative distribution of attenuation derived from emission measurements.

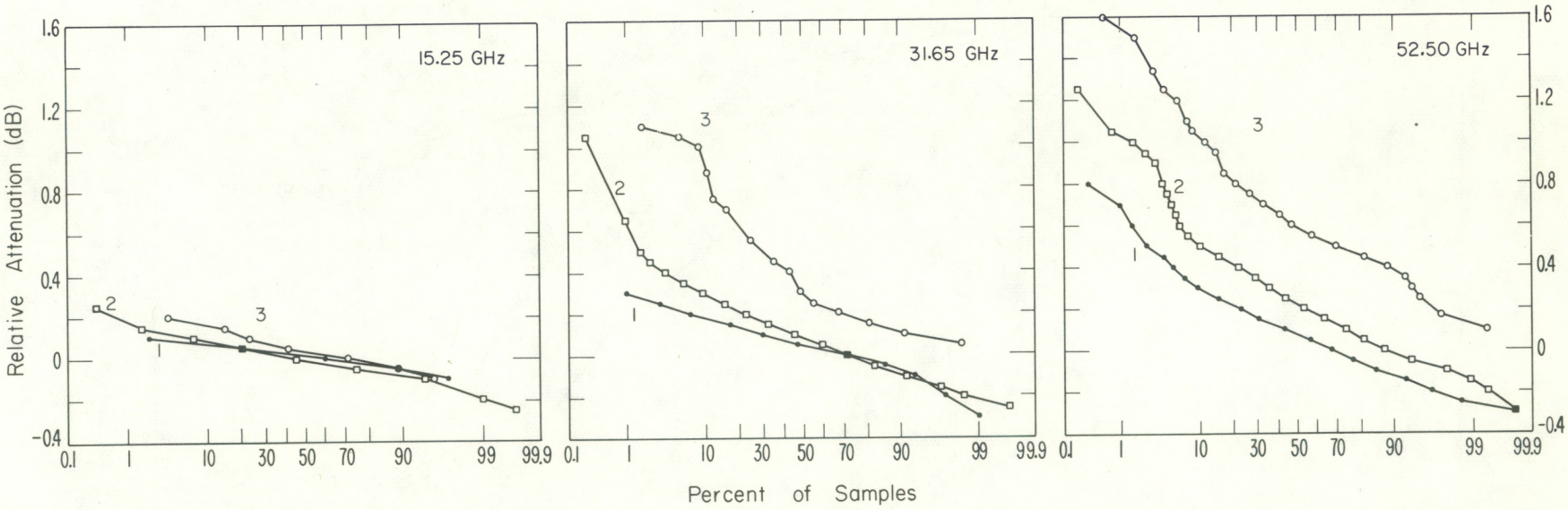

Figure B-1. Cumulative distribution of attenuation relative to clear air. Numbers on curves refer to sky codes.

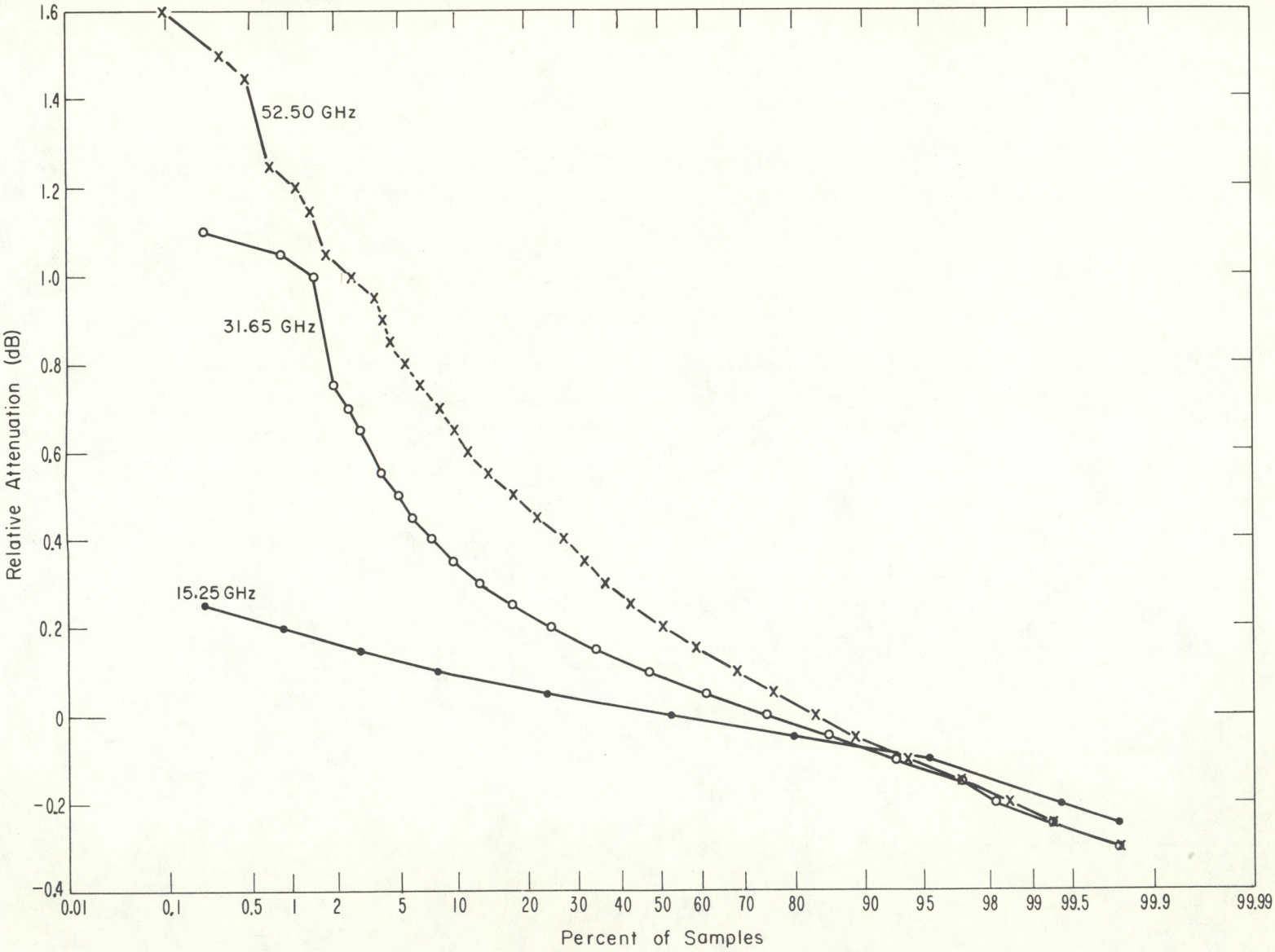

Figure B-2. Cumulative distribution of attenuation relative to clear air.

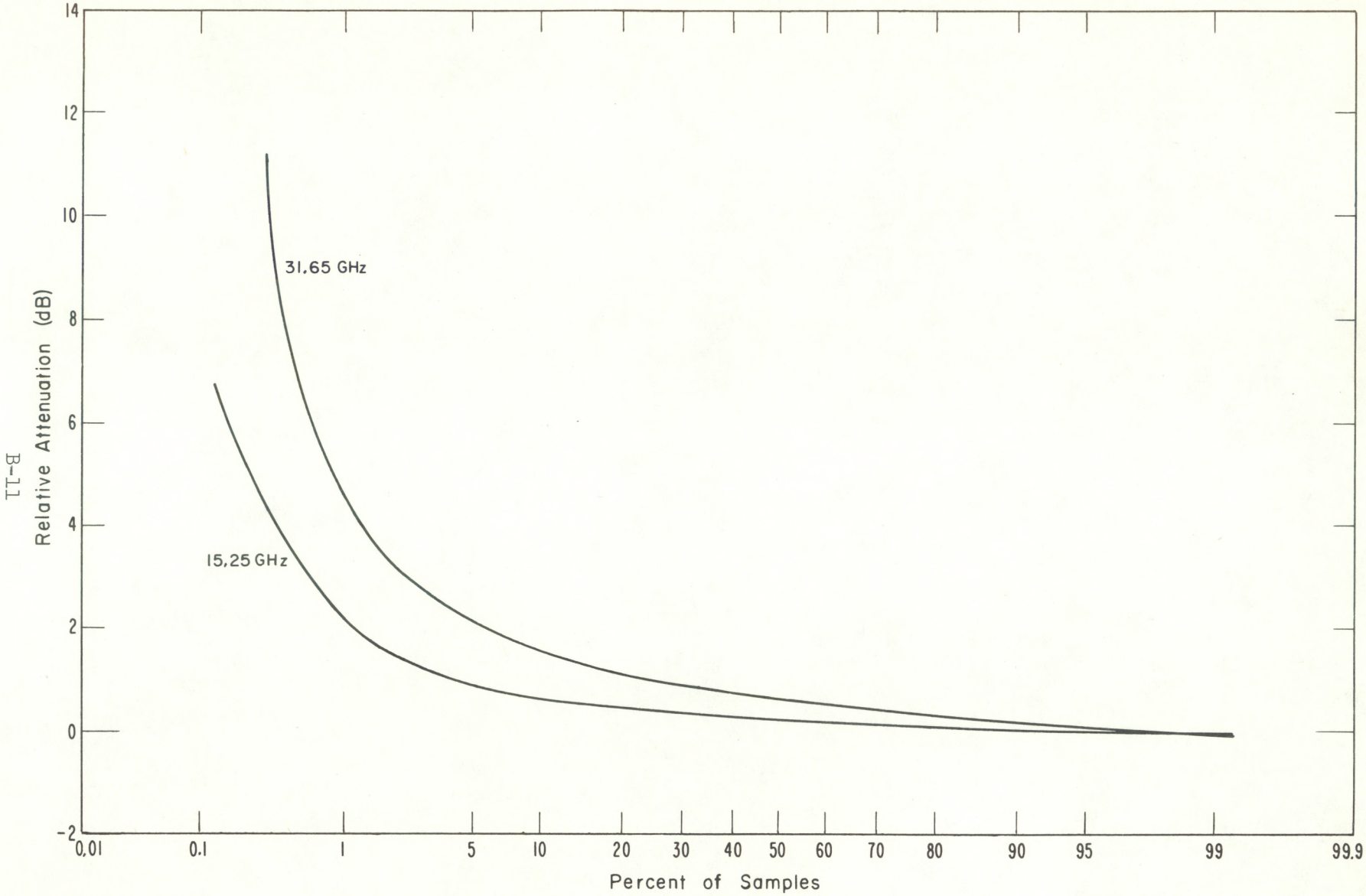

Figure B-3. Cumulative distribution of attenuation derived from emission measurements.

APPENDIX C

ABSORPTION BY TWO-COMPONENT ICE-WATER SPHERES IN THE RAYLEIGH REGION

The Rayleigh absorption coefficient for a two-component sphere was given in section 4 as

$$\alpha = \frac{1.885}{\lambda} \quad I\{-K\} \quad , \tag{C1}$$

where

$$K(\varepsilon_1, \varepsilon_2, q) = \frac{(\varepsilon_2 - 1)(\varepsilon_1 + 2\varepsilon_2) + q^3(2\varepsilon_2 + 1)(\varepsilon_1 - \varepsilon_2)}{(\varepsilon_2 + 2)(\varepsilon_1 + 2\varepsilon_2) + q^3(2\varepsilon_2 - 2)(\varepsilon_1 - \varepsilon_2)} \quad . \tag{C2}$$

Calculations of α for ε_1 = ice and ε_2 = water showed that $\alpha_{2\text{-comp}}$ was greater than α water. Since ice is essentially non-absorbing, it is quite surprising that a sphere with an interior of ice, and hence a smaller amount of absorber, can have a larger absorption than a sphere composed entirely of water. It has been shown by Battan et al., [1970] that the Mie attenuation cross section of an ice coated sphere is much larger than that of an equivalent mass of ice, but comparison with the all water case was not done. In our work, we present a simple physical mechanism for the above results, and present calculations for the ice-water and water-ice spheres.

The basic premise is the following: the two-component ice-water sphere has a larger absorption than the corresponding water sphere because of an electric field distortion in which the energy of the incident wave is concentrated in the lossy (water) portion of the sphere. In the reverse water-ice sphere, the field lines tend to resemble those of a single water sphere of radius reduced by a factor of q.

In the Rayleigh region, the particle size is much smaller than the wavelength of the incident wave and the instantaneous field that it experiences is uniform over its extent. The solution for the electric field distribution can hence be obtained by considering the equivalent electrostatic problem. This approach for the single component sphere is discussed by Kerker [1969]. We consider a two-component non-conducting dielectric sphere of inner and outer radius a and b, with dielectric constants ε_1 and ε_2. The dielectric external to the sphere is ε_3. It is assumed that $\sqrt{\varepsilon_1}\, a / 2\pi\lambda$ and $\sqrt{\varepsilon_2}\, b / 2\pi\lambda$ are much less than unity. The electrostatic potential problem can be solved in the usual way [Jackson, 1962] to yield the internal and external electric field, $\vec{E}$

$$\vec{E} = \frac{9\,\varepsilon_2\,\varepsilon_3\,\varepsilon_1}{2\,q^3\,(\varepsilon_2 - \varepsilon_1)(\varepsilon_3 - \varepsilon_2) + (\varepsilon_1 + 2\varepsilon_2)(\varepsilon_2 + 2\varepsilon_3)}\,\vec{k}\,, \qquad (C3)$$

for $r \leq a$

$$\vec{E} = \frac{3\varepsilon_3 (2\varepsilon_2 + \varepsilon_1) E_0}{2q^3 (\varepsilon_2 - \varepsilon_1)(\varepsilon_3 - \varepsilon_2) + (\varepsilon_1 + 2\varepsilon_2)(\varepsilon_2 + 2\varepsilon_3)} \vec{k}$$

$$+ a^3 \frac{3\varepsilon_3 (\varepsilon_2 - \varepsilon_1) E_0}{2q^3 (\varepsilon_2 - \varepsilon_1)(\varepsilon_3 - \varepsilon_2) + (\varepsilon_1 + 2\varepsilon_2)(\varepsilon_2 + 2\varepsilon_3)} \left\{ \frac{\vec{k}}{r^3} - \frac{3\cos\theta \vec{r}}{r^4} \right\}, \quad (C4)$$

for $a \leq r \leq b$,

and

$$\vec{E} = - b^3 \frac{(\varepsilon_1 + 2\varepsilon_2)(\varepsilon_2 - \varepsilon_3) + q^3(\varepsilon_1 - \varepsilon_2)(\varepsilon_3 + 2\varepsilon_2) E_0}{2q^3 (\varepsilon_2 - \varepsilon_1)(\varepsilon_3 - \varepsilon_2) + (\varepsilon_1 + 2\varepsilon_2)(\varepsilon_2 + 2\varepsilon_3)} \left\{ \frac{\vec{k}}{r^3} - \frac{3\cos\theta \vec{r}}{r^4} \right\}$$

$$+ E_0 \vec{k} \quad , \quad (C5)$$

for $r \geq b$.

Above, the incident field, E_0, is in the z direction specified by the unit vector, $\vec{k}$, $\vec{r}$ is the distance vector from the origin to the field point, and θ is the polar angle measured with respect to the z axis. The electric displacement vector is obtained from $\vec{D} = \varepsilon \vec{E}$.

Electric displacement field lines were generated for the ice-water and water-ice spheres using the real part of the dielectric constants given in section 4 and (C3), (C4), and (C5). A particular

field line was determined by integrating a differential equation whose slope is determined from the field lines. For example,

$$dy = \frac{D_y}{D_z}\, dz \quad , \tag{C6}$$

and

$$ds^2 = dx^2 + dy^2 + dz^2 \quad . \tag{C7}$$

A planar cross section of $\vec{D}$ field lines is shown in figure C-1 for $\lambda = 10$ cm and $q = 0.9$. It is evident by inspection that the field lines tend to lie in the water shell in the ice-water sphere and tend to closely resemble those of a one-component water sphere of reduced radius in the water-ice case. The latter is in qualitative agreement with figure 6, which shows that the attenuation of the water-ice sphere increases almost directly with q.

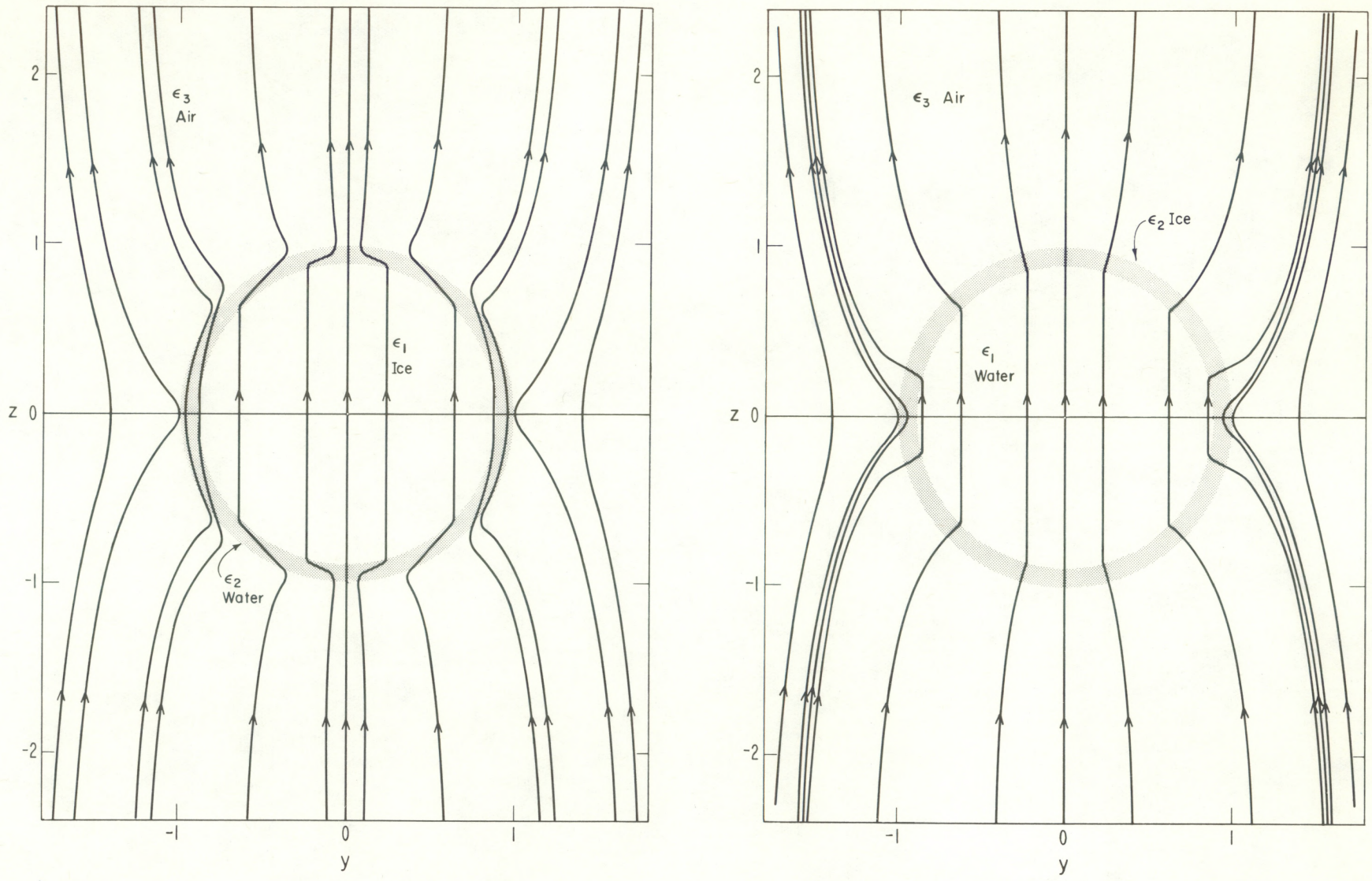

Figure C-1. $\vec{D}$ field lines for water-ice spheres.

REFERENCES

Battan, L. J., S. R. Browning and B. M. Herman (1970), Attenuation of microwaves by wet ice spheres, J. Appl. Meteor. 9, 832-834.

Jackson, J. D. (1962), Classical Electrodynamics, J. Wiley & Sons, Inc., New York, New York.

Kerker, Milton (1969), The Scattering of Light and Other Electromagnetic Radiation, Academic Press, New York, New York.